Author Manuscript

Author Manuscript

Author Manuscript

Author Manuscript

HHS Public Access

Author manuscript

Dev Neurobiol. Author manuscript; available in PMC 2017 October 01.

Published in final edited form as:

Dev Neurobiol. 2016 October ; 76(10): 1160–1181. doi:10.1002/dneu.22382.

Distinct Intracellular Signaling Mediates C-MET Regulation of Dendritic Growth and Synaptogenesis

Kathie L. Eagleson[1,*], **Christianne J. Lane**[2], **Lisa McFadyen-Ketchum**, **Sara Solak**, **Hsiao-Huei Wu**[1], and **Pat Levitt**[1,3]

[1]Department of Pediatrics, Children's Hospital Los Angeles, Keck School of Medicine, University of Southern California, Los Angeles, CA

[2]Divison of Biostatistics, Department of Preventive Medicine, Keck School of Medicine, University of Southern California

[3]Institute for the Developing Mind, The Saban Research Institute, Children's Hospital Los Angeles, Keck School of Medicine, University of Southern California, Los Angeles, CA

Abstract

Hepatocyte growth factor (HGF) activation of the MET receptor tyrosine kinase influences multiple neurodevelopmental processes. Evidence from human imaging and mouse models shows that, in the forebrain, disruptions in MET signaling alter circuit formation and function. One likely means of modulation is by controlling neuron maturation. Here, we examined the signaling mechanisms through which MET exerts developmental effects in the neocortex. In situ hybridization revealed that *hgf* is located near MET-expressing neurons, including deep neocortical layers and periventricular zones. Western blot analyses of neocortical crude membranes demonstrated that HGF-induced MET autophosphorylation peaks during synaptogenesis, with a striking reduction in activation between P14 and P17 just prior to pruning. In vitro analysis of postnatal neocortical neurons assessed the roles of intracellular signaling following MET activation. There is rapid, HGF-induced phosphorylation of MET, ERK1/2 and Akt that is accompanied by two major morphological changes increases in total dendritic growth and synapse density. Selective inhibition of each signaling pathway altered only one of the two distinct events. MAPK/ERK pathway inhibition significantly reduced the HGF-induced increase in dendritic length, but had no effect on synapse density. In contrast, inhibition of the PI-3K/Akt pathway reduced HGF-induced increases in synapse density, with no effect on dendritic length. The data reveal a key role for MET activation during the period of neocortical neuron growth and synaptogenesis, with distinct biological outcomes mediated via discrete MET-linked intracellular signaling pathways in the same neurons.

Keywords

neocortex; ERK; Akt; HGF; neuronal differentiation

[*]Kathie Eagleson Ph.D., The Saban Research Institute, Children's Hospital Los Angeles, 4650 Sunset Blvd, MS #135, Los Angeles, CA 90027, keagleso@med.usc.edu.

The authors declare no competing financial interests.

Author Manuscript Author Manuscript Author Manuscript Author Manuscript

INTRODUCTION

Signaling via the MET receptor influences multiple neurodevelopmental processes, with outcomes dependent upon cell context and stage of development (Bertotti and Comoglio, 2003). It is not surprising, therefore, that alterations in MET expression have been associated with neurodevelopmental disorders, including autism spectrum disorder (ASD) (Campbell et al., 2006; Voineagu et al., 2011; Peng et al., 2013) and Rett Syndrome (Plummer et al., 2013), although the cellular mechanisms underlying this association are only beginning to be elucidated. It is becoming increasingly evident, however, that disruptions in synapse development and function are common features of neurodevelopmental disorders, with many identified risk genes having demonstrated roles in these processes (Qiu et al., 2012; Zoghbi and Bear, 2012; Castro et al., 2013). In this context, there is accumulating evidence that MET signaling impacts circuit development in the forebrain through its modulation of dendritic growth and synapse formation. A comprehensive map of MET transcript and protein expression in the mouse forebrain revealed that MET is enriched in neocortex, hippocampus and subcortical limbic regions, with expression peaking during the period of process outgrowth and synaptogenesis and waning during synapse refinement (Judson et al., 2009; Judson et al., 2011; Qiu et al., 2014). Further, over this period, MET is expressed almost exclusively in excitatory projection neurons (Eagleson et al., 2011) and is enriched in both pre- and postsynaptic compartments (Eagleson et al., 2013). Comparative analyses in primate confirmed the conservation of MET expression temporally, with peak levels observed during axon outgrowth and synapse formation, indicating a similar developmental role in the rodent and primate forebrain. Interestingly, there are evolutionary differences at the circuit level, with MET enriched in primate hippocampal CA1 neurons and temporal, posterior parietal and occipital neocortical regions, but absent in frontal lobe (Judson et al., 2011; Mukamel et al., 2011). In vitro, addition of the MET ligand, hepatocyte growth factor (HGF), increases clustering of postsynaptic proteins, modulates synapse function and regulates dendritic growth of hippocampal and neocortical pyramidal neurons (Akimoto et al., 2004; Gutierrez et al., 2004; Tyndall and Walikonis, 2006; Lim and Walikonis, 2008; Finsterwald and Martin, 2011). Following *Met* deletion in vivo, alterations in spine size and dendritic arborization, as well as increased local excitatory drive on neocortical projection neurons and premature maturation of CA1 hippocampal circuits, are consistent with altered excitatory synapse development and function (Judson et al., 2010; Qiu et al., 2011; Qiu et al., 2014).

Upon activated HGF binding, MET dimerizes, resulting in autophosphorylation of tyrosine residues in the catalytic domain (Longati et al., 1994) and phosphorylation of additional tyrosine residues located in the multi-substrate docking site in the C-terminal domain (Ponzetto et al., 1994). This leads to the activation of multiple downstream intracellular signaling pathways, including phosphatidylinositol-3 kinase (PI-3 K)/Akt and ERK/MAPK. The outcomes of the intracellular signaling via MET activation result in diverse, cell- and context-dependent cellular responses (e.g. (Borowiak et al., 2004; Brusevold et al., 2012; Chang et al., 2012)). Both pathways have been implicated in modulating dendritic growth and synapse formation (e.g. (Lim and Walikonis, 2008; Giachello et al., 2010; Finsterwald and Martin, 2011; Majumdar et al., 2011)), but there is a knowledge gap in determining the

Author Manuscript Author Manuscript Author Manuscript Author Manuscript

discrete events that each pathway mediates when activated in the same neuron. In the present study, we demonstrate that, during the early stage of synaptogenesis, activated MET (pMET) is enriched in neocortical neuropil, but is largely absent in developing white matter, where MET expression is highest. Consistent with this, *hgf* transcript is also detected in the neocortical neuropil. Using crude membrane preparations, we demonstrate that peak MET activation in response to HGF in the neocortex occurs during the first two postnatal weeks, followed by a significant decline in HGF-induced activation near the onset of pruning in the 3rd postnatal week. Further, in primary cultures of neocortical neurons, the increase in synapse number in response to HGF requires activation of the PI-3K/Akt pathway, whereas the increase in dendritic length requires activation of the ERK/MAPK pathway.

MATERIALS AND METHODS

Animals

Timed-pregnant C57Bl/6 mice were purchased from The Jackson Laboratory. All research procedures using mice were approved by the Institutional Animal Care and Use Committee at the University of Southern California and at Children's Hospital Los Angeles and conformed to NIH guidelines. Mice were housed under a 12 hour light-dark cycle, with food and water ad libitum.

Immunohistochemistry

P7 mice were anesthetized with sodium pentobarbital (100mg/kg i.p.) and perfused with 4% paraformaldehyde in phosphate-buffered saline. The brains were removed, postfixed and processed for immunohistochemistry as described previously (Judson et al., 2009), using rabbit anti-phospho-MET (Tyr1234/1235) (pMET, 1:150) or mouse anti-MET (1:250, Santa Cruz Biotechnology) on adjacent sections. Incubation with unlabeled donkey anti-mouse IgG Fab fragments was omitted for the pMET immunostaining only.

Crude membrane preparations

Male and female mice were decapitated under isoflurane anesthesia (Western Medical Supply) and the neocortex dissected. Unless otherwise noted, all subsequent steps were performed at 4°C and reagents were supplied by Sigma. To compare the kinetics of MET activation across development, fresh tissue from 4 pups was pooled at each age (multiple time points between P0–28) and homogenized as described previously (Judson et al., 2009). The homogenate was centrifuged at 1,000g for 15 minutes to remove nuclei and cell debris. The resulting supernatant was centrifuged at 16,000g for 15 minutes to yield a pellet containing a crude membrane fraction, which was resuspended in artificial cerebrospinal fluid (125mM NaCl, 2.5mM KCL, 1.0mM KH_2PO_4, 2.5mM $CaCl_2$, 1.0mM $MgCl_2$, 26mM $NaHCO_3$ and 10mM dextrose, pH 7.4) saturated with 95% O_2 and 5% CO_2. The pooled samples were then aliquoted and a sample of each aliquot was removed for protein quantification using the BCA protein assay kit (BioRad). Preparations were stimulated at 37°C with 0 or 50ng/ml recombinant mouse HGF for 1–10 minutes. To compare the magnitude of MET activation across development, in a second set of experiments crude neocortical membranes were prepared from 4 (P0), 2 (P7) or 1 (>P7) pups and stimulated as described above for 1 minute. At the end of the stimulation period, final sample buffer was

Author Manuscript Author Manuscript Author Manuscript Author Manuscript

added to the aliquot at a final concentration of 1X (12mM Tris HCl pH 6.8, 5% glycerol, 0.4% SDS, 2.8mM 2-mercaptoethanol and 0.02% bromophenol blue), the samples boiled for 5 minutes and stored at −20°C until analyzed by Western blot.

In situ hybridization

P14 mouse brains were fresh-frozen in ice-cold isopentane and sectioned in the coronal plane at 25 μm. Sections were subjected to in situ hybridization as previously described (Wu and Levitt, 2013) using a digoxigenin-labeled cRNA mouse *hgf* probe (176–966 and 1189–1816bp of GenBank No. AK042121). Control probe of 760 bases of antisense to neomycin phosphotransferase gene transcripts (*neo*) was generated from pSPT-Neo control plasmid provided in Roche DIG RNA Labeling Kit (Cat. No. 11175025910). The color reaction was performed at room temperature with BM purple (Roche). Images were acquired using a Zeiss Axio Observer Inverted microscope with a motorized stage and Zeiss AxioCam MRm camera (Carl Zeiss), using Zeiss Axiovision 4.1 software (Carl Zeiss).

Neuron cultures

Primary cultures of neocortical neurons were prepared from P1 mice according to a published protocol (Beaudoin et al., 2012), with the following minor modifications. For immunocytochemical analyses, individual cultures were generated from a single pup (3 – 4 male or female pups/culturing session) and neurons plated at 750 cells/mm^2 on 12mm glass coverslips (Carolina Biological) in 24-well dishes. Note that neither a glial feeder layer nor glial conditioned medium was used, which slows the process of synapse maturation in these cultures. The neurons remain healthy for at least 20 days in vitro (DIV), the longest that we have monitored them. To facilitate analyses, at 5 DIV, neurons were transfected at low efficiency with a GFP-expressing plasmid (PCAGGS-eGFP, obtained from Dr. Le Ma, Thomas Jefferson School of Medicine) using the Calcium Phosphate for Mammalian Cells Transfection Kit (Clonetech) according to manufacturer's instructions. This resulted in the transfection of 25 – 30 neurons per coverslip. For biochemical analyses, tissue from a single litter (5–6 male and female pups) was pooled and neurons plated at the same density in 6-well plates. At 13–14 DIV, HGF was added to the medium at 50ng/ml final concentration and incubated at 37°C for either 1–60 minutes (biochemistry) or 24 hours (immunocytochemistry). In some experiments, cultures were treated with the MAPK/ERK inhibitors PD 98059 (25μM, Millipore) and PD 184352 (1μM, Sigma), the PI3K/Akt inhibitors wortmannin (100nM, Millipore) and PI 828 (3μM, R&D Systems), or vehicle (DMSO) for 30 minutes prior to and during HGF treatment. At the concentrations used here, treatment with either inhibitor alone, without HGF addition, did not have any significant effect on morphology or synapse density.

For immunocytochemical analyses, coverslips were fixed first with 4% paraformaldehyde in phosphate buffered saline (PBS) for 15 minutes at 4°C, followed by pre-chilled methanol for 10 minutes at 4°C. Next, coverslips were washed sequentially with PBS and PBST (0.05% Triton-X in PBS), each for 15 minutes at room temperature, then blocked in 5% fetal bovine serum in PBST for 1 hour at room temperature. The coverslips were incubated overnight at 4°C in the following cocktail of primary antibodies: mouse anti-PSD95 (1:1,000, Pierce Biotechnology), rabbit anti-synapsin 1 (1:1,000, Cell Signaling) and chick anti-green

Author Manuscript Author Manuscript Author Manuscript Author Manuscript

fluorescent protein (GFP, 1:1,000, Abcam). Following three 15-minute washes in PBS, coverslips were incubated for 1 hour at room temperature in a cocktail of Alexa Fluor-conjugated secondary antibodies (Life Technologies): goat anti-mouse 633, goat anti-rabbit 546, and goat anti-chick 488, all at 1:1,000. Coverslips were washed three times for 15 minutes in PBS, mounted with ProLong Gold (Life Technologies), and stored at 4°C until imaging.

For biochemical analyses, wells were washed twice with PBS, and incubated on ice for 5 minutes in Laemmli buffer (63mM Tris HCl pH 6.8, 10% glycerol, 2% SDS) with 50mM DTT. The cells were scraped from the wells, transferred to a tube and left standing on ice for 15 minutes, vortexing briefly every 5 minutes. Samples were centrifuged at 4°C for 10 minutes at 10,000g, the supernatant collected and stored at −80°C until analyzed by Western blot.

Western blot analysis

SDS-PAGE and Western blotting were performed as described previously (Eagleson et al., 2013), with the following modifications. For both crude membrane and in vitro assays, samples covering the entire time course undergoing the same treatment were analyzed on duplicate blots to measure the kinetics of activation following addition of HGF. The blots were probed sequentially with the following primary antibodies (except where noted, antibodies are from Cell Signaling): 1) blot 1 - rabbit anti-phospho-MET (Tyr1234/1235) (pMET, 1:1,000), mouse anti-MET (1:500, Santa Cruz Biotechnology), rabbit anti-phospho-p44/42 MAPK (Thr202/Tyr204) (pERK, 1:1,000) and rabbit anti-p44/42 MAPK (ERK, 1:10,000); and 2) blot 2 - rabbit anti-phospho-Akt (Thr308) ($pAkt^{308}$, 1:250), mouse anti-phospho-Akt (Ser473) ($pAkt^{473}$, 1:500) and rabbit anti-Akt (1:10,000). For both blots, mouse anti-α-tubulin (1:100,000, EMD Millipore) confirmed equal protein loading and transfer. Species appropriate horseradish peroxidase-conjugated secondary antibodies (Jackson Immunoresearch,) were used at 1:5,000. To compare the magnitude of MET activation across development, samples from each age stimulated with HGF for 1 minute were analyzed on the same blot and probed for pMET and total MET. Because α-tubulin expression changes over the first four weeks of development, equal protein loading and transfer were confirmed with the Pierce Reversible Protein Stain Kit (ThermoFisher). Immunoreactive bands were visualized with Pierce SuperSignal West Dura Chemiluminescent Substrate (Thermo Scientific), with the exception of $pAkt^{308}$ and $pAkt^{473}$, which used Pierce SuperSignal West Femto Chemiluminescent Substrate (Thermo Scientific). Image capture and densitometric analysis was performed using a CCD camera coupled to a UVP BioImaging System using VisionWorksLS Image Acquisition and Analysis software (v. 7.0.1, VisionWorks). After the density of each band was measured, a global background subtraction was applied and, at each time point, a ratio of phosphorylated to total protein was generated and normalized to the untreated sample.

Neuron image analysis

For each set of coverslips generated from a single pup, ten transfected neurons with a pyramidal morphology were imaged in each treatment group for analysis. In a pilot study, using data generated in a previous publication (Wang et al., 2015), we determined that 8 – 10

Author Manuscript Author Manuscript Author Manuscript Author Manuscript

neurons was sufficient to reflect stably the average synapse density per coverslip (Supplementary Figure 1), with no differences when analyzing additional neurons/coverslip. Cell sampling was done by making non-overlapping, vertical sweeps of the coverslip in the GFP channel. Images were performed on single neurons, where the dendritic processes had not contacted those of a neighboring GFP-labeled neuron and exhibited the morphology of a pyramidal neuron. The individuals capturing the images and performing the analyses were blinded to the treatment group. To measure synapse density, a subfield of the proximal dendritic tree was imaged. Fluorescent-labeled images were captured on a LSM 710 confocal microscope (Zeiss) using a 63X oil objective lens. Neuron imaging was optimized for obtaining synapse and dendritic measures. The parameters were adjusted to maintain the signal level within the dynamic range, remained unchanged for all images collected. Images were converted to TIFF files, imported into Image J, and synaptic density determined using an automated custom Image J plug-in for synapse identification that was developed in our laboratory (https://github.com/Pat-Levitt/SynapseCounter; (Wang et al., 2015)). For each image, the custom Image-J plug-in first counted the number of PSD-95 clusters that have congruent signal with GFP-labeled dendrites. Those PSD-95 clusters that co-localized with synapsin-1 were then defined as a synapse. For dendritic length and number of branch point measurements, images of the entire dendritic tree were acquired with a Zeiss AxioCam MRm camera in Axiovision (v 4.1) and both parameters measured with Image J software. For each treatment group, synaptic density, dendritic length and number of branch points were averaged across the ten neurons sampled to produce a single value for each pup, with each pup considered an independent sample.

Statistical analysis

Sample size varied between studies and is indicated in the figure legends. For analyses involving crude membrane preparations, comparisons between conditions were made using repeated measures ANCOVA models. The within subjects factor was time, while age and treatment were between groups factors. When sphericity assumptions could not be met according to Mauchley's test for sphericity, Greenhouse-Geisser adjustments for df were made in order to avoid type I error. For analyses using primary neuron cultures, comparisons between groups were performed using a two-way ANOVA (morphological measures), a repeated measures two-way ANOVA (Western blot measures – kinetics of activation), or a one-way ANOVA (Western blot measures – levels of pMET and MET across development). If significant differences were observed, these analyses were complemented with the Tukey's HSD (honest significant difference) test to identify the source of possible interactions. For some analyses, in which only two groups were being compared, a two-tailed t-test was used. Effect sizes from pilot experiments supported the expectation for moderate to large effects of HGF on dendritic length, number of branch points and synapse density (Cohen, 1988). A power analysis indicated that a total sample of 7 (dendritic length and number of branch points) and 6 (synapse density) would be required to detect such effects with 90% power and alpha at 0.05. For all tests, p values are reported to the third decimal place. Analyses were performed with SPSS (v.21); *a priori* $\alpha = 0.05$.

Author Manuscript Author Manuscript Author Manuscript Author Manuscript

Digital illustrations

Graphs were prepared in SigmaPlot (v. 7.0, SPSS). Images and graphs were converted to TIFF format and imported into Adobe Photoshop CS5 (v. 12.1), in which they were cropped, resized and adjusted for brightness and contrast for preparation of final figures.

RESULTS

MET activation in the neocortex peaks during the period of synaptogenesis

We previously demonstrated that total MET expression in the neocortex is relatively low during the later periods of embryonic development, increasing markedly over the first postnatal week to reach peak levels between P7 – P14 (Judson et al., 2009). Subsequently, there is a gradual decline in MET expression through the onset of puberty, with a low baseline expression level maintained in the adult. During the peak period of expression, MET protein is expressed heavily in developing axon tracts, including the corpus callosum and anterior commissure, with lower levels of expression in the developing neuropil ((Judson et al., 2009); Figure 1A). In contrast, activated MET (pMET) is relatively low to absent in white matter, but is expressed at high levels in the cortical gray matter, notably superficial layers and layer V (Figure 1B). The spatial mismatch between the gradients of MET and pMET expression could be due to 1) the ratio of internalized to surface MET in different cell compartments; for example, in axon tracts, MET signal may reflect receptor undergoing anterograde transport to axon terminals. In this scenario, only surface MET would have access to HGF; 2) the ratio of unprocessed precursor protein to the mature, signaling-competent form of MET, both of which are recognized by the antibody; or 3) the distribution of HGF across the forebrain.

We next measured whether the timing of MET activation in crude neocortical membranes after ligand addition changes over development. At all ages analyzed, we detected the mature, signaling-competent form of MET (145kD), but not the unprocessed precursor protein (170kD, Figure 1C). To determine levels of pMET, we used an antibody that specifically detects the receptor when it is phosphorylated at Tyr1234/1235. Phosphatase inhibitors were not included in the crude membrane preparations, and thus the basal levels of pMET without ligand are low (Figure 1C) and do not reflect the phosphorylation status in vivo. Typically, at all ages following addition of HGF, there is an increase in pMET that can be observed as early as 1 minute post-treatment (Figure 1C – E). At P0 and P10, this is followed by a decrease in pMET at the 5 and 10 minute time points (Figure 1C, D). At P7, corresponding to the early period of synaptogenesis in the neocortex, the activation peak is broader, either remaining elevated for 5 minutes (2 of 4 samples) or increasing further (2 of 4 samples) before decreasing by 10 minutes. In contrast, at later ages, pMET levels over the assay period are similar to that observed at 1 minute (Figure 1E). Sphericity cannot be assumed in this sample (Mauchley's test for sphericity $p < 0.001$) and, given the small sample size, the more conservative Greenhouse-Geisser adjustment to the df was made for reporting of results. There is a significant interaction effect of age (P0-P28) and stimulation time (1–10 minutes), $F_{16.1, 42.9} = 5.4$, $p < .001$, on the ratio of pMET to total MET. Further, there is a significant main effect of treatment time [$F_{1.8, 42.9} = 28.0$, $p < .001$]. Finally, there is a significant main effect of age [$F_{9, 24} = 7.1$, $p < .001$]. Post-hoc analyses revealed the

Author Manuscript Author Manuscript Author Manuscript Author Manuscript

specific ages between which significant differences in MET activation were observed (Table 1). In a second set of experiments, crude membrane preparations at each age were stimulated with HGF for 1 minute and levels of MET and pMET were processed on the same blot (Figure 1F, G). There was a significant effect of age on the levels of MET ($F_{7, 16} = 18.4$, $p < .001$) and pMET ($F_{7, 16} = 37.7$, $p < .001$). Post-hoc analyses revealed the specific ages between which significant differences in MET (Table 2) and pMET (Table 3) levels were observed. The temporal pattern observed is consistent with a role for MET in mediating early dendritic growth and synapse formation. Given that the mature, signaling-competent form of MET predominates, these data, taken together, suggest that the spatial mismatch between MET and pMET arises because of the differential availability of HGF or the internal localization of MET within the axonal compartment.

The results of the experiments above raise the question of potential sources of HGF *in vivo*. We addressed this using in situ hybridization to map *hgf* expression in the mouse telencephalon at P14, the peak of synaptogenesis. At this age, expression of *hgf* transcript was observed in discrete regions (Figure 2). There was robust signal in periventricular zones (Figure 2A, A'), consistent with previous studies in adult rat reporting expression of HGF protein and message in the ependyma (Jung et al., 1994; Hayashi et al., 1998). In the neocortex, *hgf* transcript labeling is most evident in deep, rather than superficial, layers (Figure 2A, B, B'), with a consistent lateral to medial gradient. Hippocampal *hfg* labeling is largely limited to CA3 (Figure 2C, C'), complementary to *Met* expression which is almost exclusively in CA1 neurons (Judson et al., 2009). Finally, we note two additional areas exhibiting heavy labeling: the indusium griseum (Figure 2B), located below the anterior and posterior cingulate cortices, that expresses *Met*, and the basolateral amygdala (Figure 2C), in which *Met* is located in medial and cortical regions. No signal was observed in adjacent sections when using a control probe against *neo*, a bacterial gene (Supplementary Figure 2).

HGF modulates dendritic growth and synapse formation in neocortical neurons

The dynamic profile of HGF-induced activation of MET across neocortical development suggests that the neurodevelopmental processes most likely to be impacted by this signaling system are dendritic growth and synapse formation. Because the *in vivo* data following *Met* genetic deletion are correlative (Judson et al., 2010), we investigated the morphological impact of receptor activation directly using primary cultures of neocortical neurons. First, we confirmed that the MET receptor was activated in response to HGF at 13 DIV (Figure 3A, B). Similar to the crude membrane preparations, we detected the processed form of MET (145kD), but not the unprocessed precursor protein (170kD). Further, following addition of HGF, there is a rapid increase in pMET that can be observed as early as 1 minute post-treatment and remains elevated for the length of the assay period (Figure 3A, B), similar to the crude membranes prepared after P10. Statistical analyses revealed that the main effect of HGF treatment (0 and 50ng/ml) was significant [$F_{1, 44} = 10.2$, $p=0.019$], as was the main effect of treatment time [0–120 minutes, $F_{11, 44} = 2.6$, $p=0.014$]. Further, there was a significant interaction between HGF presence and treatment time [$F_{11, 44} = 2.6$, $p=0.013$]. Next, dendritic length, number of branch points, and synapse density were measured at 13–14 DIV following stimulation with HGF for 24 hours, with data generated from 7 pups over 2 independent culturing sessions. Neurons were transfected with a GFP-

Author Manuscript Author Manuscript Author Manuscript Author Manuscript

expressing plasmid at 5 DIV, permitting the entire dendritic arbor to be imaged and reconstructed (Figure 3C). One day post-treatment, there was already a significant increase in dendritic length ($t_{12} = -6.15$, $p<0.001$, Figure 3D) and number of branch points ($t_{12} = -4.67$, $p<0.001$, Figure 3E) in neurons treated with HGF (length: 1296.60μm [95% CI: 1288.67, 1364.53], branch points: 12.02 [95% CI: 10.24, 13.80]) compared to untreated controls (length: 965.56μm [95% CI: 884.87, 1046.25], branch points: 7.14 [95% CI: 6.13, 8.15]), consistent with a previous report *in vitro* (Finsterwald and Martin, 2011). Synaptic density also was measured in a subfield of the GFP-labeled proximal dendritic tree using a customized plug-in developed in our laboratory (Wang et al., 2015). Within 24 hr of HGF addition, there was a significant increase in synaptic density ($t_{12} = -2.74$, $p=0.012$, Figure 3G), defined by co-localization of synapsin-1 and PSD-95 (Figure 3F), following HGF stimulation (untreated: 2.81/100μm^2 [95% CI: 2.20, 3.42], HGF: 4.54/100μm^2 [95% CI: 3.47, 5.61]).

Inhibition of the ERK/MAPK pathway prevents HGF-induced dendritic growth, but not synapse formation

It was reported that the ERK/MAPK pathway mediates HGF-induced dendritic growth in cortical neurons at 3DIV (Finsterwald and Martin, 2011). In pilot studies, we found that ERK1/2 was phosphorylated in response to HGF in the crude membrane preparations (data not shown). We first confirmed that ERK1/2 was activated in response to HGF at 13 DIV. In Western blots, two bands were detected at 44 and 42kD, representing ERK1 and ERK2 respectively (Figure 4A). Phosphorylation of both was observed 5 minutes post-treatment and remained elevated for the assay period (60 minutes, Figure 4A, B). We therefore investigated whether this pathway is similarly involved in dendritic growth at 14 DIV and, further, if ERK/MAPK activation mediates synapse formation. To determine the role of this pathway, cultures were treated with PD98059 or PD184352, selective inhibitors of MAPK kinase that prevents the downstream phosphorylation of ERK1/2(Dudley et al., 1995; Sebolt-Leopold et al., 1999). The dose of inhibitor was selected on the basis of a pilot dose-response study (PD98059 – 25μM, Figure 4C; PD184352 – 1μM, Figure 4D), which revealed nearly undetectable levels of pERK except at the lowest concentration of each inhibitor.

We next measured the effects of each inhibitor on HGF-induced dendritic growth (Figure 5). For PD98059 (Figure 5A–B), there was a significant main effect of HGF treatment on total dendritic length [$F_{1, 24} = 11.2$, $p=0.003$], but there was no main effect of inhibitor ($F_{1, 24} = 2.2$, $p=0.151$). There was also a significant interaction between HGF treatment and inhibitor ($F_{1, 24} = 5.9$, $p=0.003$). Post-hoc analyses using Tukey's HSD (Table 4) indicated that the vehicle + HGF group (1342.98μm, [95% CI: 1205.98, 1479.98]) had longer total dendritic lengths than each of the other three groups (vehicle alone: 1029.42μm [95% CI: 956.76, 1102.08]; PD98059 alone: 1080.47μm [95% CI: 994.04, 1166.90]; PD98059 + HGF: 1130.57μm [95% CI: 1013.02, 1248.12]) and that the HGF effect was observed in the presence of vehicle but not inhibitor. For PD184352 (Figure 5D), there was no main effect of HGF treatment on total dendritic length [$F_{1, 24} = 3.9$, $p=0.059$], but there was a significant main effect of inhibitor ($F_{1, 24} = 5.0$, $p=0.035$). There was also a significant interaction between HGF treatment and inhibitor ($F_{1, 24} = 5.6$, $p=0.026$]. Post-hoc analyses using

Author Manuscript Author Manuscript Author Manuscript Author Manuscript

Tukey's HSD (Table 4) indicated that the vehicle + HGF group (1409.95μm, [95% CI: 1239.45, 1580.45]) had longer total dendritic lengths than the other three groups (vehicle alone: 1076.86μm [95% CI: 934.05, 1219.67]; PD184352 alone: 1087.08μm [95% CI: 955.25, 1218.91]; PD184352 + HGF: 1056.90μm [95% CI: 905.34, 1208.46]) and that the inhibitor effect was only observed in HGF, but not non-HGF, treated cultures.

We measured the number of branch points as another indicator of dendritic growth. For PD98095 (Figure 5C), there was a significant main effect of HGF treatment on the number of branch points [$F_{1, 24} = 16.2$, $p<0.001$] and a significant main effect of inhibitor ($F_{1, 24} = 13.7$, $p=0.001$) on the number of branch points. There was also a significant interaction between HGF treatment and PD98059 [$F_{1, 24} = 22.5$, $p<0.001$]. Post-hoc analyses using Tukey's HSD (Table 5) indicated that the vehicle + HGF group (11.70, [95% CI: 10.41, 12.99]) had a higher number of branch points than each of the other three groups (vehicle alone: 7.66 [95% CI: 6.95, 8.37]; PD98059 alone: 8.14 [95% CI: 7.55, 8.73]; PD98059 + HGF: 7.80 [95% CI: 6.95, 8.68]). Further, the HGF effect was only observed in the presence of vehicle and the effect of the inhibitor was only observed in HGF-treated cultures. For PD184352 (Figure 5E), there was a significant main effect of HGF treatment ($F_{1, 24} = 5.4$, $p = 0.029$], but no main effect of inhibitor ($F_{1, 24} = 2.4$, $p=0.136$) on the number of branch points. There was also a significant interaction between HGF treatment and inhibitor [$F_{1, 24} = 4.4$, $p<0.047$]. Post-hoc analyses using Tukey's HSD (Table 5) indicated that the vehicle + HGF group (12.59 [95% CI: 10.35, 14.83]) had a higher number of branch points than the other three groups (vehicle alone: 8.71 [95% CI: 7.11, 10.31]; PD184352 alone: 9.20 [95% CI: 7.72, 10.68]; PD184352 + HGF: 9.40 [95% CI: 7.96, 10.84]) and that the inhibitor effect was observed only in HGF, but not non-HGF, treated cultures.

Finally, we measured the effects of both MAPK kinase inhibitors on HGF-induced synapse density (Figure 6). For PD98059 (Figure 6B), there was a significant main effect of HGF treatment on synapse density [$F_{1, 24} = 14.4$, $p=0.001$], but there was no main effect of inhibitor ($F_{1, 24} = 0.4$, $p=0.518$). Further, there was no significant interaction between HGF treatment and inhibitor [$F_{1, 24} = 0.6$, $p=0.465$]. These results indicate that HGF treatment increased synaptic density in both vehicle- (vehicle alone: 3.43/100μm^2 [95% CI: 2.73, 4.13]; vehicle + HGF: 6.02/100μm^2 [95% CI: 4.61, 7.43]) and PD98059- (PD98059 alone: 3.48/100μm^2 [95% CI: 2.61, 4.35]; PD98059 + HGF: 5.22/100μm^2 [95% CI: 3.88, 6.56]) treated cultures. For PD184352 (Figure 6A, C), there was a significant main effect of HGF treatment on synapse density [$F_{1, 24} = 14.4$, $p=0.001$], but there was no main effect of inhibitor ($F_{1, 24} = 0.4$, $p=0.518$). Further, there was no significant interaction between HGF treatment and inhibitor [$F_{1, 24} = 0.6$, $p=0.465$]. These results indicate that HGF treatment increased synaptic density in both vehicle- (vehicle alone: 3.96/100μm^2 [95% CI: 2.80, 5.12]; vehicle + HGF: 6.57/100μm^2 [95% CI: 5.24, 7.90]) and PD184352- (PD184352 alone: 3.88/100μm^2 [95% CI: 3.29, 4.47]; PD184352 + HGF: 6.71/100μm^2 [95% CI: 5.69, 7.73]) treated cultures. Together, these results indicate that activation of the ERK/MAPK pathway is required for the positive effect of HGF on dendritic growth, but has no impact on the HGF-induced increase in synapse density.

Author Manuscript Author Manuscript Author Manuscript Author Manuscript

Inhibition of the PI-3K/Akt pathway prevents HGF-induced synapse formation, but not dendritic growth

Both the ERK/MAPK and PI-3K/Akt pathways have been implicated in synapse formation in response to a variety of signals (Giachello et al., 2010; Majumdar et al., 2011; Khan et al., 2013) and Akt is phosphorylated in response to HGF in the crude membrane preparations (data not shown) and *in vitro* (Figure 7A, B). Because HGF-induced activation of the ERK/MAPK pathway did not modulate synapse density, we reasoned that activation of the PI-3K/Akt pathway may be required for HGF-mediated synapse development. To test this hypothesis, we first confirmed that Akt was activated in response to HGF at 13 DIV. In Western blots, a single band was detected at ~60kD (Figure 7A). Phosphorylation at Thr308 ($pAkt^{308}$) and Ser473 ($pAkt^{473}$) could be observed as early as 1 minute post-treatment and remained elevated for the assay period (60 minutes, Figure 7A, B). To determine the role of this pathway, cultures were treated with wortmannin or PI 828, selective inhibitors of PI-3K that prevents the downstream phosphorylation of Akt (Powis et al., 1994; Gharbi et al., 2007). The dose of inhibitor was selected on the basis of a pilot dose-response study (wortmannin – 100nM, Figure 4C; PI 828 – 3μM, Figure 7D) that revealed nearly undetectable pAkt phosphorylation at the two residues using these and higher concentrations.

We next measured the effects of each inhibitor on HGF-induced dendritic growth (Figure 8). For wortmannin (Figure 8 A, B), there was a significant main effect of HGF treatment (0 or 50ng/ml) on total dendritic length ($F_{1, 24} = 13.6$, p=0.001), but there was no main effect of inhibitor ($F_{1, 24} = 0.6$, p=0.453). Further, there was no significant interaction between HGF treatment and inhibitor [$F_{1, 24} = 0.1$, p=0.813]. These results indicate that HGF treatment increased dendritic length in both vehicle- (vehicle alone: 867.35μm [95% CI: 697.87, 1036.83]; vehicle + HGF: 1185.26μm [95% CI: 1056.15, 1314.37]) and wortmannin- (wortmannin alone: 948.50μm [95% CI: 828.34, 1068.66]; wortmannin + HGF: 1227.64μm [95% CI: 1024.94, 1430.34]) treated cultures. For PI 828 (Figure 8D), there was a significant main effect of HGF treatment (0 or 50ng/ml) on total dendritic length ($F_{1, 24} = 16.3$, $p < 0.001$), but there was no main effect of inhibitor ($F_{1, 24} = 0.5$, p=0.476). Further, there was no significant interaction between HGF treatment and inhibitor ($F_{1, 24} = 0.1$, p=0.790). These results indicate that HGF treatment increased dendritic length in both vehicle- (vehicle alone: 1076.86μm [95% CI: 934.05, 1219.67]; vehicle + HGF: 1409.95μm, [95% CI: 1239.45, 1580.45]) and PI 828- (PI 828 alone: 1041.76μm [95% CI: 908.65, 1174.87]; PI 828 + HGF: 1333.25μm [95% CI: 1176.60, 1489.90]) treated cultures.

We measured the number of branch points as another indicator of dendritic growth. For wortmannin (Figure 6C), there was a significant main effect of HGF treatment (0 or 50ng/ml) on number of branch points ($F_{1, 24} = 36.5$, p<0.001), but there was no main effect of inhibitor ($F_{1, 24} = 1.4$, p=0.256). Further, there was no significant interaction between HGF treatment and inhibitor [$F_{1, 24} = 0.0$, p=0.984]. These results indicate that HGF treatment increased the number of branch points in both vehicle- (vehicle alone: 7.87 [95% CI: 6.61, 9.13]; vehicle + HGF: 12.24 [95% CI: 10.83, 13.65]) and wortmannin- (wortmannin alone: 8.70 [95% CI: 6.96, 10.44]; wortmannin + HGF: 13.10 [95% CI: 11.89, 14.31]) treated cultures. For PI 828 (Figure 8E), there was a significant main effect of HGF

Author Manuscript Author Manuscript Author Manuscript Author Manuscript

treatment (0 or 50ng/ml) on number of branch points ($F_{1, 24} = 116.5$, $p < 0.001$), but there was no main effect of inhibitor ($F_{1, 24} = 0.0$, p=0.988). Further, there was no significant interaction between HGF treatment and inhibitor [$F_{1, 24} = 0.1$, p=0.798]. These results indicate that HGF treatment increased the number of branch points in both vehicle- (vehicle alone: 8.71 [95% CI: 7.11, 10.31]; vehicle + HGF: 12.59, [95% CI: 10.35, 14.83]) and PI 828- (PI 828 alone: 8.46 [95% CI: 7.02, 9.90]; PI 828 + HGF: 12.78 [95% CI: 10.89, 14.67]) treated cultures.

Finally, we measured the effects of both PI-3K inhibitors on the HGF-induced increase synapse density (Figure 9). For wortmannin (Figure 9B), there was a significant main effect of HGF treatment ($F_{1, 24} = 6.4$, p=0.019) and a significant main effect of inhibitor ($F_{1, 24} = 6.6$, p=0.017) on synapse density. Further, there was a significant interaction between HGF treatment and inhibitor [$F_{1, 24} = 7.2$, p=0.013]. Post-hoc analyses using Tukey's HSD tests (Table 6) showed that the vehicle + HGF group (6.11/100μm^2 [95% CI: 4.69, 7.53]) had greater synapse density than each of the other three groups (vehicle alone: 3.34/100μm^2 [95% CI: 2.44, 4.24]; wortmannin alone: 3.40/100μm^2 [95% CI: 2.37, 4.43]; wortmannin + HGF: 3.31/100μm^2 [95% CI: 2.69, 3.93]). Further, the HGF effect was only observed in the presence of vehicle and the effect of the inhibitor was only observed in HGF-treated cultures. For PI 828 (Figure 9A, C), there was no main effect for HGF treatment ($F_{1, 24} = 8.1$, p=0.062), but there was a significant main effect of inhibitor ($F_{1, 24} = 13.5$, p=0.019] on synapse density. Further, there was a significant interaction between HGF treatment and inhibitor [$F_{1, 24} = 10.4$, p=0.036]. Post-hoc analyses using Tukey's HSD tests (Table 6) showed that the vehicle + HGF group (6.57/100μm^2 [95% CI: 5.24, 7.90]) had greater synapse density than each of the other three groups (vehicle alone: 3.96/100μm^2 [95% CI: 2.80, 5.12]; PI 828 alone: 4.11/100μm^2 [95% CI: 3.23, 4.99]; PI 828 + HGF: 4.27/100μm^2 [95% CI: 3.38, 5.16]). Further, the HGF effect was only observed in the presence of vehicle and the effect of the inhibitor was only observed in HGF-treated cultures. Together, these results indicate that activation of the PI-3K/Akt pathway is required for the effect of HGF on synapse density, but not for HGF-induced dendritic growth.

DISCUSSION

In the present study, we used biochemical and morphological analyses to demonstrate that two discrete intracellular signaling pathways underlie distinct HGF-induced biological outcomes in developing neocortical neurons. Further, we identify a key developmental epoch, corresponding to the period of dendritic outgrowth and synaptogenesis, during which HGF stimulation elicits maximal activation of MET in the neocortex.

Methodological considerations

In the current study, we used small-molecule inhibitors to dissect the effects of the PI3-K/Akt and MAPK/ERK pathways in mediating the biological outcomes of MET signaling in neocortical neurons. In cell-based assays, LY294002 and wortmannin are the most widely used inhibitors of PI3-K. Thus, we used wortmannin at a concentration (100nM), which does not inhibit any non-target kinases in a panel of kinases (Davies et al., 2000; Bain et al., 2007), and PI 828, a more potent analogue of LY294002 (Gharbi et al., 2007). Several small-

Author Manuscript Author Manuscript Author Manuscript Author Manuscript

molecule inhibitors for the MAPK pathways have been developed, including PD98059 and PD184352, which inhibit MEK1/2, thus preventing phosphorylation of ERK1/2 (Dudley et al., 1995; Sebolt-Leopold et al., 1999). Some studies indicate that PD98059 can also inhibit MEK5 (Karihaloo et al., 2001; Mody et al., 2001), and we cannot exclude the possibility that the effects of this inhibitor on HGF-induced dendritic growth may be mediated, at least in part, by ERK5. The second MAPK pathway inhibitor used in this study, PD184352, is reported to have enhanced selectivity and potency compared to PD98059 (Allen et al., 2003). It should be noted that low levels of ERK and Akt phosphorylation could be detected at the concentration of inhibitors used, particularly when the blots were exposed for more extended periods. Higher doses of drug, however, produced toxic effects in the neuron cultures. As inhibition of each pathway had distinct effects on HGF-induced synapse formation and dendritic growth in developing neocortical neurons, it is unlikely that the drugs had gross off target effects. The results are consistent with each intracellular signaling pathway mediating distinct components of neuronal differentiation.

Our culture system using primary postnatal neocortical neurons is a modification of a published protocol (Beaudoin et al., 2012). The basal synapse density reported here is lower than that in some other studies. It is important to emphasize, however, that lower synaptic density does not reflect the health of the neurons at the time of the assay (13–14DIV; see Supplementary Figure 3), as we have monitored such cultures for up to 21 DIV without noticeable neuron loss. Rather, synapse density reflects two parameters: 1) the absence of a glial feeder layer or glial conditioned medium - under these conditions, synapse maturation is slowed, and we have shown here that it can be enhanced by HGF stimulation of MET; and 2) our automated analysis system expresses synapse density per unit area of dendrite, including spines, as defined by the GFP signal, rather than the tradition per unit length.

Finally, with regard to our experimental design, pilot studies revealed a moderate to large effect of HGF on dendritic growth and synapse density and a subsequent power analysis indicated that a sample size of 6 and 7, respectively, would be sufficient to detect such effects with 90% power and alpha at 0.05. In the current study, for statistical purposes, we consider cultures generated from a single animal as an independent sample. We note that when the same statistical analyses were performed with each neuron considered an independent sample (n = 70/group), the outcomes were the same.

Mechanisms of MET-Mediated Neuronal Differentiation

In the developing nervous system, HGF-induced activation of MET leads to diverse biological outcomes that are dependent on cell context and developmental stage. For example, HGF/MET signaling modulates proliferation of cerebellar granule cell precursors (Ieraci et al., 2002), axon outgrowth and survival of subpopulations of motor (Ebens et al., 1996; Caton et al., 2000; Koyama et al., 2003; Lamballe et al., 2011) and sympathetic (Thompson et al., 2004) neurons, and the migration of olfactory interneurons (Garzotto et al., 2008). In contrast, MET signaling appears to have no impact on proliferation or survival in the developing telencephalon (Judson et al., 2010). Rather, accumulating evidence from morphological and electrophysiological studies in genetically manipulated animal models and from human imaging studies indicates that, in the cortex, MET signaling influences

Author Manuscript Author Manuscript Author Manuscript Author Manuscript

circuit maturation (Qiu et al., 2011; Hedrick et al., 2012; Qiu et al., 2014). The present study, together with previous analyses examining effects of MET activation (Gutierrez et al., 2004; Tyndall and Walikonis, 2006; Nakano et al., 2007; Lim and Walikonis, 2008; Judson et al., 2010; Finsterwald and Martin, 2011; Qiu et al., 2011; Qiu et al., 2014), suggest that the results from both human and animal models *in vivo* are likely due to MET's effects on dendritic and spine morphogenesis, and synapse development. Neuronal growth and synaptogenesis occur over an extended period of time. The present study addresses the elements of HGF activation of MET that change over time and, to our knowledge, for the first time discriminates the intracellular mediators of MET activation that control distinct aspects of neocortical neuronal differentiation. The biochemical analyses demonstrate that the peak in HGF-induced MET activation corresponds to P7 – P14, the peak period of synaptogenesis and dendritic outgrowth in the mouse neocortex, declining abruptly between P14 and P17, when pruning and functional synapse maturation occurs. Of interest is that reducing or deleting *Met* expression by various methods in vivo results in premature hippocampal synapse maturation(Qiu et al., 2014), suggesting that MET may serve as a temporal regulator of this complex process of forming and stabilizing synapses.

The analyses of HGF-induced MET signaling in crude membrane preparations raised the question of potential sources of endogenous HGF *in vivo*. Both pre- and post-synaptic sources of ligand have been reported for receptor tyrosine kinases in the nervous system. In the hippocampus, TrkB signaling modulates synaptic formation and plasticity in response to presynaptic and postsynaptic release of BDNF (Dean et al., 2012; Dieni et al., 2012; Andreska et al., 2014; Edelmann et al., 2015). Our data suggest a presynaptic release mechanism may operate for hippocampal HGF/MET signaling, as *hgf* is expressed by CA3 neurons, which project to MET-expressing CA1 neurons, whose development is disrupted by increasing or decreasing MET expression (Qiu et al., 2014). We also identified a source for HGF that is intrinsic to the neocortex, with expression largely limited to deep layers, consistent with a role for MET signaling in the physiological maturation of interlaminar local circuits (Qiu et al., 2011). The present data do not distinguish whether neocortically derived HGF is released pre- or post-synaptically to activate MET. It is interesting to note, however, that in the frontal cortex, there is increased excitatory drive from layer II/III neurons onto layer V neurons in the absence of MET signaling (Qiu et al., 2011); in this context, layer V neurons potentially would act as a postsynaptic source of HGF for MET-expressing layer II/III neurons early in synapse formation. The periventricular source of *hgf* could potentially bathe the forebrain in HGF during the peak of synapse formation and dendritic growth, or have more local effects. This will require more examination.

While many of the mechanisms that underlie the MET response diversity at different developmental stages are not fully understood, downstream signaling pathways, co-operative signaling with other receptors, and the modulatory effects of interacting proteins may be particularly important. Previous studies mostly focus on a single biological outcome when assessing the contribution of individual intracellular signaling pathways to HGF/MET signaling. There is more limited information available on potential differential roles of two primary intracellular targets of MET activation in the same cells. Often, both the ERK and PI3/Akt pathways are activated in response to HGF, but the requirement for these pathways is only examined narrowly in terms of cellular impact. For example, inhibition of PI3K/Akt

Author Manuscript Author Manuscript Author Manuscript Author Manuscript

pathway shows that it is required for HGF-dependent motility in mouse hepatocellular carcinoma cells (Li et al., 2013), and the neuroprotective effect of HGF on cerebellar granule neurons under excitotoxic conditions *in vitro* (Hossain et al., 2002). Potential functional outcomes of HGF-induced MAPK/ERK activation were not examined in those studies. In some instances, it appears that only one pathway is selectively activated in response to HGF. For example, in the rostral migratory stream, migration of olfactory interneurons is modulated by HGF, which activates the MAPK/ERK, but not the PI3K/Akt, pathway (Garzotto et al., 2008). In the present study, experiments were designed to address the role of MAPK/ERK and PI3K/Akt signaling in mediating two primary HGF-induced biological responses, dendritic outgrowth and synapse formation, within the same cell population and at the same time in development. We focused on these pathways for three reasons. First, activation of both pathways has been implicated in dendritic outgrowth and synapse formation in the neocortex and hippocampus in response to a variety of stimuli, including estrogen, insulin and BDNF (Alonso et al., 2004; Lee et al., 2011; Khan et al., 2013; Sellers et al., 2015). Second, HGF-induced activation of ERK1/2 and Akt in neocortical neurons *in vitro* has been reported (He et al., 2008; Finsterwald and Martin, 2011). *In vitro* studies showed that activation of both pathways mediates the neuroprotective effects of HGF following hypoxia (He et al., 2008). HGF-induced dendritic outgrowth requires the MAPK/ERK pathway *in vitro*, whereas inhibition of the PI3K/Akt pathway had no effect (Finsterwald and Martin, 2011). The latter study additionally identified CREB phosphorylation and the subsequent interaction of CREB with CRTC1 as a requirement for the effects of HGF on dendritic growth, but did not perform experiments to determine the outcomes mediated by activation of PI3K/Akt in the same neurons. Third, both pathways were activated in response to HGF in our neocortical crude membrane preparations and in the postnatal neocortical neuron cultures. We confirmed the requirement for the MAPK/ERK pathway in mediating HGF-induced dendritic outgrowth in neocortical neurons. The experiments further demonstrate that HGF-induced synapse formation in the same cell population requires activation of the PI3K/Akt pathway, but not ERK/MAPK. In contrast, Lim and colleagues (Lim and Walikonis, 2008) reported that the modulatory effects of HGF on dendritic morphogenesis in hippocampal neurons are dependent on activation of Akt. The role of the MAPK/ERK pathway, however, was not measured in their study. All evidence thus far supports the hypothesis that HGF-mediated MET signaling is highly context dependent, which is necessary to produce a similar biological effect in different neuron populations (Bertotti and Comoglio, 2003).

The present results begin to reveal how dendritic growth and synapse formation in response to HGF might be independently regulated. This may be particularly important in discrete neocortical neuron populations at different developmental times. One possibility is that, in certain contexts, activation of the MAPK/ERK or PI3K/Akt pathway may be favored, perhaps due to the interacting proteins that are co-expressed at a particular time in development. For example, there is increasing evidence that MET-interacting receptors, including neuropilins (Matsushita et al., 2007; Prud'homme and Glinka 2012) and semaphorins (Giordano et al., 2002), can influence activation of MET and, thus, biological outcomes in response to HGF. Alternatively, mediation could occur via regulation of downstream effectors. For example, in Madin-Darby canine kidney cells, ephrin-A1

Author Manuscript Author Manuscript Author Manuscript Author Manuscript

suppressed HGF-induced branching through suppression of Rac1 and p21-activated kinase activation (Miao et al., 2003). We are in the process of identifying MET-interacting proteins in developing neocortical synaptosomes (Xie, Li, Baker, Coba and Levitt, unpublished observations). These studies may reveal potential mediators of differential signaling in distinct neuron subpopulations that express different interacting proteins. While remaining a significant challenge to the field, the present study provides a conceptualization of how data from human genetic, neuroimaging and mouse models may be translated to determine mechanisms of neurobiological vulnerability that lead to neurodevelopmental disorders.

Supplementary Material

Refer to Web version on PubMed Central for supplementary material.

Acknowledgments

This work was supported by National Institute of Mental Health R01 MH067842 and the Simms/Mann Chair in Developmental Neurogenetics (P.L.), and by NIH/NCRR SC CTSI UL1TR000130. Its contents are solely the responsibility of the authors and do not necessarily represent the official views of the NIH. We thank Rebecca Southern for excellent technical assistance and Matthew Judson for the immunocytochemical analyses.

REFERENCES

Akimoto M, Baba A, Ikeda-Matsuo Y, Yamada MK, Itamura R, Nishiyama N, Ikegaya Y, Matsuki N. Hepatocyte growth factor as an enhancer of nmda currents and synaptic plasticity in the hippocampus. Neuroscience. 2004; 128:155–162. [PubMed: 15450362]

Allen LF, Sebolt-Leopold J, Meyer MB. CI-1040 (PD184352), a targeted signal transduction inhibitor of MEK (MAPKK). Semin Oncol. 2003; 30:105–116. [PubMed: 14613031]

Alonso M, Medina JH, Pozzo-Miller L. ERK1/2 activation is necessary for BDNF to increase dendritic spine density in hippocampal CA1 pyramidal neurons. Learn Mem. 2004; 11:172–178. [PubMed: 15054132]

Andreska T, Aufmkolk S, Sauer M, Blum R. High abundance of BDNF within glutamatergic presynapses of cultured hippocampal neurons. Front Cell Neurosci. 2014; 8:107. [PubMed: 24782711]

Bain J, Plater L, Elliott M, Shpiro N, Hastie CJ, McLauchlan H, Klevernic I, Arthur JS, Alessi DR, Cohen P. The selectivity of protein kinase inhibitors: a further update. Biochem J. 2007; 408:297–315. [PubMed: 17850214]

Beaudoin GM 3rd, Lee SH, Singh D, Yuan Y, Ng YG, Reichardt LF, Arikkath J. Culturing pyramidal neurons from the early postnatal mouse hippocampus and cortex. Nat Protoc. 2012; 7:1741–1754. [PubMed: 22936216]

Bertotti A, Comoglio PM. Tyrosine kinase signal specificity: lessons from the HGF receptor. Trends Biochem Sci. 2003; 28:527–533. [PubMed: 14559181]

Borowiak M, Garratt AN, Wustefeld T, Strehle M, Trautwein C, Birchmeier C. Met provides essential signals for liver regeneration. Proc Natl Acad Sci U S A. 2004; 101:10608–10613. [PubMed: 15249655]

Brusevold IJ, Aasrum M, Bryne M, Christoffersen T. Migration induced by epidermal and hepatocyte growth factors in oral squamous carcinoma cells in vitro: role of MEK/ERK, p38 and PI-3 kinase/Akt. J Oral Pathol Med. 2012; 41:547–558. [PubMed: 22413835]

Campbell DB, Sutcliffe JS, Ebert PJ, Militerni R, Bravaccio C, Trillo S, Elia M, Schneider C, Melmed R, Sacco R, Persico AM, Levitt P. A genetic variant that disrupts MET transcription is associated with autism. Proc Natl Acad Sci U S A. 2006; 103:16834–16839. [PubMed: 17053076]

Castro J, Mellios N, Sur M. Mechanisms and therapeutic challenges in autism spectrum disorders: insights from Rett syndrome. Curr Opin Neurol. 2013; 26:154–159. [PubMed: 23449173]

Author Manuscript Author Manuscript Author Manuscript Author Manuscript

Caton A, Hacker A, Naeem A, Livet J, Maina F, Bladt F, Klein R, Birchmeier C, Guthrie S. The branchial arches and HGF are growth-promoting and chemoattractant for cranial motor axons. Development. 2000; 127:1751–1766. [PubMed: 10725250]

Chang CC, Chiu JJ, Chen SL, Huang HC, Chiu HF, Lin BH, Yang CY. Activation of HGF/c-Met signaling by ultrafine carbon particles and its contribution to alveolar type II cell proliferation. Am J Physiol Lung Cell Mol Physiol. 2012; 302:L755–L763. [PubMed: 22245998]

Cohen, J. Statistical power analysis for the behavioral neurosciences. Hillsdale, New Jersey: Lawrence Erlbaum Associates; 1988.

Davies SP, Reddy H, Caivano M, Cohen P. Specificity and mechanism of action of some commonly used protein kinase inhibitors. Biochem J. 2000; 351:95–105. [PubMed: 10998351]

Dean C, Liu H, Staudt T, Stahlberg MA, Vingill S, Buckers J, Kamin D, Engelhardt J, Jackson MB, Hell SW, Chapman ER. Distinct subsets of Syt-IV/BDNF vesicles are sorted to axons versus dendrites and recruited to synapses by activity. J Neurosci. 2012; 32:5398–5413. [PubMed: 22514304]

Dieni S, Matsumoto T, Dekkers M, Rauskolb S, Ionescu MS, Deogracias R, Gundelfinger ED, Kojima M, Nestel S, Frotscher M, Barde YA. BDNF and its pro-peptide are stored in presynaptic dense core vesicles in brain neurons. J Cell Biol. 2012; 196:775–788. [PubMed: 22412021]

Dudley DT, Pang L, Decker SJ, Bridges AJ, Saltiel AR. A synthetic inhibitor of the mitogen-activated protein kinase cascade. Proc Natl Acad Sci U S A. 1995; 92:7686–7689. [PubMed: 7644477]

Eagleson KL, Campbell DB, Thompson BL, Bergman MY, Levitt P. The autism risk genes MET and PLAUR differentially impact cortical development. Autism Res. 2011; 4:68–83. [PubMed: 21328570]

Eagleson KL, Milner TA, Xie Z, Levitt P. Synaptic and extrasynaptic location of the receptor tyrosine kinase Met during postnatal development in the mouse neocortex and hippocampus. J. Comp. Neurol. 2013

Ebens A, Brose K, Leonardo ED, Hanson MG Jr, Bladt F, Birchmeier C, Barres BA, Tessier-Lavigne M. Hepatocyte growth factor/scatter factor is an axonal chemoattractant and a neurotrophic factor for spinal motor neurons. Neuron. 1996; 17:1157–1172. [PubMed: 8982163]

Edelmann E, Cepeda-Prado E, Franck M, Lichtenecker P, Brigadski T, Lessmann V. Theta Burst Firing Recruits BDNF Release and Signaling in Postsynaptic CA1 Neurons in Spike-Timing-Dependent LTP. Neuron. 2015

Finsterwald C, Martin JL. Cellular mechanisms underlying the regulation of dendritic development by hepatocyte growth factor. Eur J Neurosci. 2011; 34:1053–1061. [PubMed: 21895802]

Garzotto D, Giacobini P, Crepaldi T, Fasolo A, De Marchis S. Hepatocyte growth factor regulates migration of olfactory interneuron precursors in the rostral migratory stream through Met-Grb2 coupling. J Neurosci. 2008; 28:5901–5909. [PubMed: 18524894]

Gharbi SI, Zvelebil MJ, Shuttleworth SJ, Hancox T, Saghir N, Timms JF, Waterfield MD. Exploring the specificity of the PI3K family inhibitor LY294002. Biochem J. 2007; 404:15–21. [PubMed: 17302559]

Giachello CN, Fiumara F, Giacomini C, Corradi A, Milanese C, Ghirardi M, Benfenati F, Montarolo PG. MAPK/Erk-dependent phosphorylation of synapsin mediates formation of functional synapses and short-term homosynaptic plasticity. J Cell Sci. 2010; 123:881–893. [PubMed: 20159961]

Gutierrez H, Dolcet X, Tolcos M, Davies A. HGF regulates the development of cortical pyramidal dendrites. Development. 2004; 131:3717–3726. [PubMed: 15229174]

Hayashi T, Abe K, Sakurai M, Itoyama Y. Inductions of hepatocyte growth factor and its activator in rat brain with permanent middle cerebral artery occlusion. Brain Res. 1998; 799:311–316. [PubMed: 9675323]

He F, Wu LX, Shu KX, Liu FY, Yang LJ, Zhou X, Zhang Y, Huang BS, Huang D, Deng XL. HGF protects cultured cortical neurons against hypoxia/reoxygenation induced cell injury via ERK1/2 and PI-3K/Akt pathways. Colloids Surf B Biointerfaces. 2008; 61:290–297. [PubMed: 17942284]

Hedrick A, Lee Y, Wallace GL, Greenstein D, Clasen L, Giedd JN, Raznahan A. Autism Risk Gene MET Variation and Cortical Thickness in Typically Developing Children and Adolescents. Autism Res. 2012

Author Manuscript Author Manuscript Author Manuscript Author Manuscript

Hossain MA, Russell JC, Gomez R, Laterra J. Neuroprotection by scatter factor/hepatocyte growth factor and FGF-1 in cerebellar granule neurons is phosphatidylinositol 3-kinase/akt-dependent and MAPK/CREB-independent. J Neurochem. 2002; 81:365–378. [PubMed: 12064484]

Ieraci A, Forni PE, Ponzetto C. Viable hypomorphic signaling mutant of the Met receptor reveals a role for hepatocyte growth factor in postnatal cerebellar development. Proc Natl Acad Sci U S A. 2002; 99:15200–15205. [PubMed: 12397180]

Judson MC, Amaral DG, Levitt P. Conserved subcortical and divergent cortical expression of proteins encoded by orthologs of the autism risk gene MET. Cereb Cortex. 2011; 21:1613–1626. [PubMed: 21127014]

Judson MC, Bergman MY, Campbell DB, Eagleson KL, Levitt P. Dynamic gene and protein expression patterns of the autism-associated met receptor tyrosine kinase in the developing mouse forebrain. J Comp Neurol. 2009; 513:511–531. [PubMed: 19226509]

Judson MC, Eagleson KL, Wang L, Levitt P. Evidence of cell-nonautonomous changes in dendrite and dendritic spine morphology in the met-signaling-deficient mouse forebrain. J Comp Neurol. 2010; 518:4463–4478. [PubMed: 20853516]

Jung W, Castren E, Odenthal M, Vande Woude GF, Ishii T, Dienes HP, Lindholm D, Schirmacher P. Expression and functional interaction of hepatocyte growth factor-scatter factor and its receptor c-met in mammalian brain. J Cell Biol. 1994; 126:485–494. [PubMed: 8034747]

Karihaloo A, O'Rourke DA, Nickel C, Spokes K, Cantley LG. Differential MAPK pathways utilized for HGF- and EGF-dependent renal epithelial morphogenesis. J Biol Chem. 2001; 276:9166–9173. [PubMed: 11118451]

Khan MM, Dhandapani KM, Zhang QG, Brann DW. Estrogen regulation of spine density and excitatory synapses in rat prefrontal and somatosensory cerebral cortex. Steroids. 2013; 78:614–623. [PubMed: 23276632]

Koyama J, Yokouchi K, Fukushima N, Kawagishi K, Higashiyama F, Moriizumi T. Neurotrophic effect of hepatocyte growth factor on neonatal facial motor neurons. Neurol Res. 2003; 25:701–707. [PubMed: 14579786]

Lamballe F, Genestine M, Caruso N, Arce V, Richelme S, Helmbacher F, Maina F. Pool-specific regulation of motor neuron survival by neurotrophic support. J Neurosci. 2011; 31:11144–11158. [PubMed: 21813676]

Lee CC, Huang CC, Hsu KS. Insulin promotes dendritic spine and synapse formation by the PI3K/Akt/mTOR and Rac1 signaling pathways. Neuropharmacology. 2011; 61:867–879. [PubMed: 21683721]

Li Y, Huang X, Zhang J, Li Y, Ma K. Synergistic inhibition of cell migration by tetraspanin CD82 and gangliosides occurs via the EGFR or cMet-activated Pl3K/Akt signalling pathway. Int J Biochem Cell Biol. 2013; 45:2349–2358. [PubMed: 23968914]

Lim CS, Walikonis RS. Hepatocyte growth factor and c-Met promote dendritic maturation during hippocampal neuron differentiation via the Akt pathway. Cell Signal. 2008; 20:825–835. [PubMed: 18262389]

Longati P, Bardelli A, Ponzetto C, Naldini L, Comoglio PM. Tyrosines1234-1235 are critical for activation of the tyrosine kinase encoded by the MET proto-oncogene (HGF receptor). Oncogene. 1994; 9:49–57. [PubMed: 8302603]

Majumdar D, Nebhan CA, Hu L, Anderson B, Webb DJ. An APPL1/Akt signaling complex regulates dendritic spine and synapse formation in hippocampal neurons. Mol Cell Neurosci. 2011; 46:633–644. [PubMed: 21236345]

Mody N, Leitch J, Armstrong C, Dixon J, Cohen P. Effects of MAP kinase cascade inhibitors on the MKK5/ERK5 pathway. FEBS Lett. 2001; 502:21–24. [PubMed: 11478941]

Mukamel Z, Konopka G, Wexler E, Osborn GE, Dong H, Bergman MY, Levitt P, Geschwind DH. Regulation of MET by FOXP2, genes implicated in higher cognitive dysfunction and autism risk. J Neurosci. 2011; 31:11437–11442. [PubMed: 21832174]

Nakano M, Takagi N, Takagi K, Funakoshi H, Matsumoto K, Nakamura T, Takeo S. Hepatocyte growth factor promotes the number of PSD-95 clusters in young hippocampal neurons. Exp Neurol. 2007; 207:195–202. [PubMed: 17678646]

Author Manuscript Author Manuscript Author Manuscript Author Manuscript

Peng Y, Huentelman M, Smith C, Qiu S. MET receptor tyrosine kinase as an autism genetic risk factor. Int Rev Neurobiol. 2013; 113:135–165. [PubMed: 24290385]

Plummer JT, Evgrafov OV, Bergman MY, Friez M, Haiman CA, Levitt P, Aldinger KA. Transcriptional regulation of the MET receptor tyrosine kinase gene by MeCP2 and sex-specific expression in autism and Rett syndrome. Transl Psychiatry. 2013; 3:e316. [PubMed: 24150225]

Ponzetto C, Bardelli A, Zhen Z, Maina F, dalla Zonca P, Giordano S, Graziani A, Panayotou G, Comoglio PM. A multifunctional docking site mediates signaling and transformation by the hepatocyte growth factor/scatter factor receptor family. Cell. 1994; 77:261–271. [PubMed: 7513258]

Powis G, Bonjouklian R, Berggren MM, Gallegos A, Abraham R, Ashendel C, Zalkow L, Matter WF, Dodge J, Grindey G, et al. Wortmannin, a potent and selective inhibitor of phosphatidylinositol-3-kinase. Cancer Res. 1994; 54:2419–2423. [PubMed: 8162590]

Qiu S, Aldinger KA, Levitt P. Modeling of autism genetic variations in mice: focusing on synaptic and microcircuit dysfunctions. Dev Neurosci. 2012; 34:88–100. [PubMed: 22572629]

Qiu S, Anderson CT, Levitt P, Shepherd GM. Circuit-specific intracortical hyperconnectivity in mice with deletion of the autism-associated Met receptor tyrosine kinase. J Neurosci. 2011; 31:5855–5864. [PubMed: 21490227]

Qiu S, Lu Z, Levitt P. MET receptor tyrosine kinase controls dendritic complexity, spine morphogenesis, and glutamatergic synapse maturation in the hippocampus. J Neurosci. 2014; 34:16166–16179. [PubMed: 25471559]

Sebolt-Leopold JS, Dudley DT, Herrera R, Van Becelaere K, Wiland A, Gowan RC, Tecle H, Barrett SD, Bridges A, Przybranowski S, Leopold WR, Saltiel AR. Blockade of the MAP kinase pathway suppresses growth of colon tumors in vivo. Nat Med. 1999; 5:810–816. [PubMed: 10395327]

Sellers KJ, Erli F, Raval P, Watson IA, Chen D, Srivastava DP. Rapid modulation of synaptogenesis and spinogenesis by 17beta-estradiol in primary cortical neurons. Front Cell Neurosci. 2015; 9:137. [PubMed: 25926772]

Thompson J, Dolcet X, Hilton M, Tolcos M, Davies AM. HGF promotes survival and growth of maturing sympathetic neurons by PI-3 kinase- and MAP kinase-dependent mechanisms. Mol Cell Neurosci. 2004; 27:441–452. [PubMed: 15555922]

Tyndall SJ, Walikonis RS. The receptor tyrosine kinase Met and its ligand hepatocyte growth factor are clustered at excitatory synapses and can enhance clustering of synaptic proteins. Cell Cycle. 2006; 5:1560–1568. [PubMed: 16861928]

Voineagu I, Wang X, Johnston P, Lowe JK, Tian Y, Horvath S, Mill J, Cantor RM, Blencowe BJ, Geschwind DH. Transcriptomic analysis of autistic brain reveals convergent molecular pathology. Nature. 2011; 474:380–384. [PubMed: 21614001]

Wang F, Eagleson KL, Levitt P. Positive regulation of neocortical synapse formation by the Plexin-D1 receptor. Brain Res. 2015

Wu HH, Levitt P. Prenatal expression of MET receptor tyrosine kinase in the fetal mouse dorsal raphe nuclei and the visceral motor/sensory brainstem. Dev Neurosci. 2013; 35:1–16. [PubMed: 23548689]

Zoghbi HY, Bear MF. Synaptic dysfunction in neurodevelopmental disorders associated with autism and intellectual disabilities. Cold Spring Harb Perspect Biol. 2012:4.

Author Manuscript
Author Manuscript
Author Manuscript
Author Manuscript

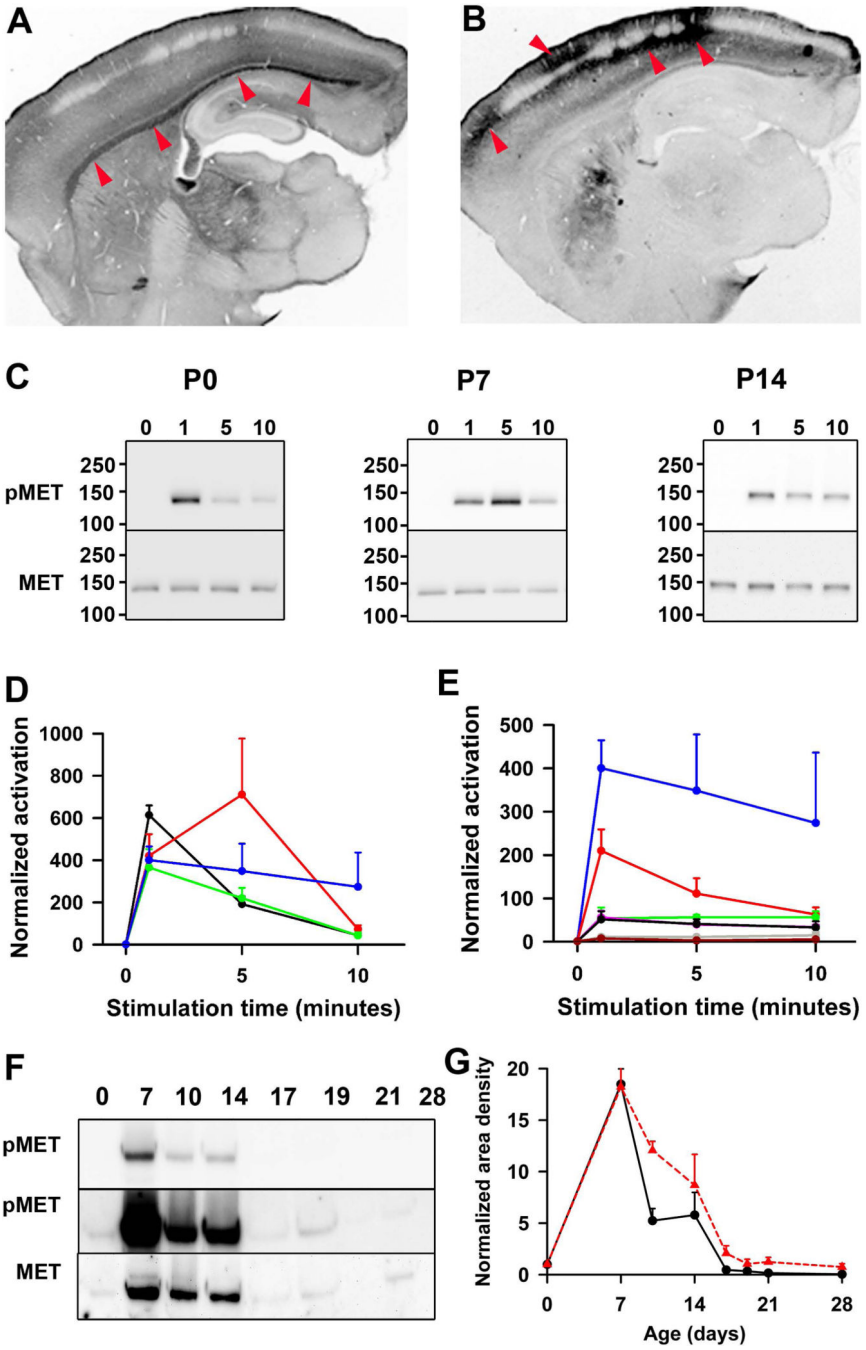

Figure 1.

A, ***B***, Photomicrographs of MET (***A***) and pMET (***B***) immunoreactivity in sagittal sections through the mouse forebrain at P7. MET is distributed throughout the neocortical neuropil and is enriched in axon tracts, including the corpus callosum (arrowheads in ***A***). There is heavy labeling of pMET in the neuropil, particularly superficial layers and layer V (arrowheads in ***B***), but pMET immunoreactivity is largely absent from axons. ***C***, Representative Western blots of MET phosphorylated at Tyr1234/1235 (pMET) following stimulation with HGF (50ng/ml) for 1–10 minutes in crude membrane preps prepared from

Author Manuscript Author Manuscript Author Manuscript Author Manuscript

the neocortex at P0, P7 and P14. ***D, E***, Quantification of the kinetics of HGF-induced MET activation in neocortex over the first and second (***D***) or third and fourth (***E***) postnatal weeks. Because each blot was processed at different times, a direct comparison of absolute values cannot be made between different ages (but see 1F,G below). Thus, pMET levels were normalized to total MET and data expressed relative to vehicle-treated samples (0). Graphs show mean pMET levels ± SEM. P14 values from the same data set are included in both graphs for comparison. ***D***, Green, P0 (N = 3 independent samples; red, P7 (N = 4); black, P10 (N = 3) and blue, P14 (N = 3). ***E***, Blue, P14; red, P17 (N = 4); green, P18 (N = 3); Pink, P19 (N = 3); black, P20 (N = 3); grey, P21 (N = 4) and brown, P28 (N = 3). ***F***, Representative Western blot of pMET and MET following stimulation with HGF (50ng/ml) for 1 minute in crude membrane preps prepared from the neocortex at different ages. Top panel shows pMET blot analyzed, while the middle panel has been exposed to show the fainter bands at P0 and older ages. ***G***, Quantification of MET (red dotted line) and HGF-induced pMET (black solid line) levels expressed relative to P0 samples. Graph shows mean ± SEM (N = 3).

Author Manuscript Author Manuscript Author Manuscript Author Manuscript

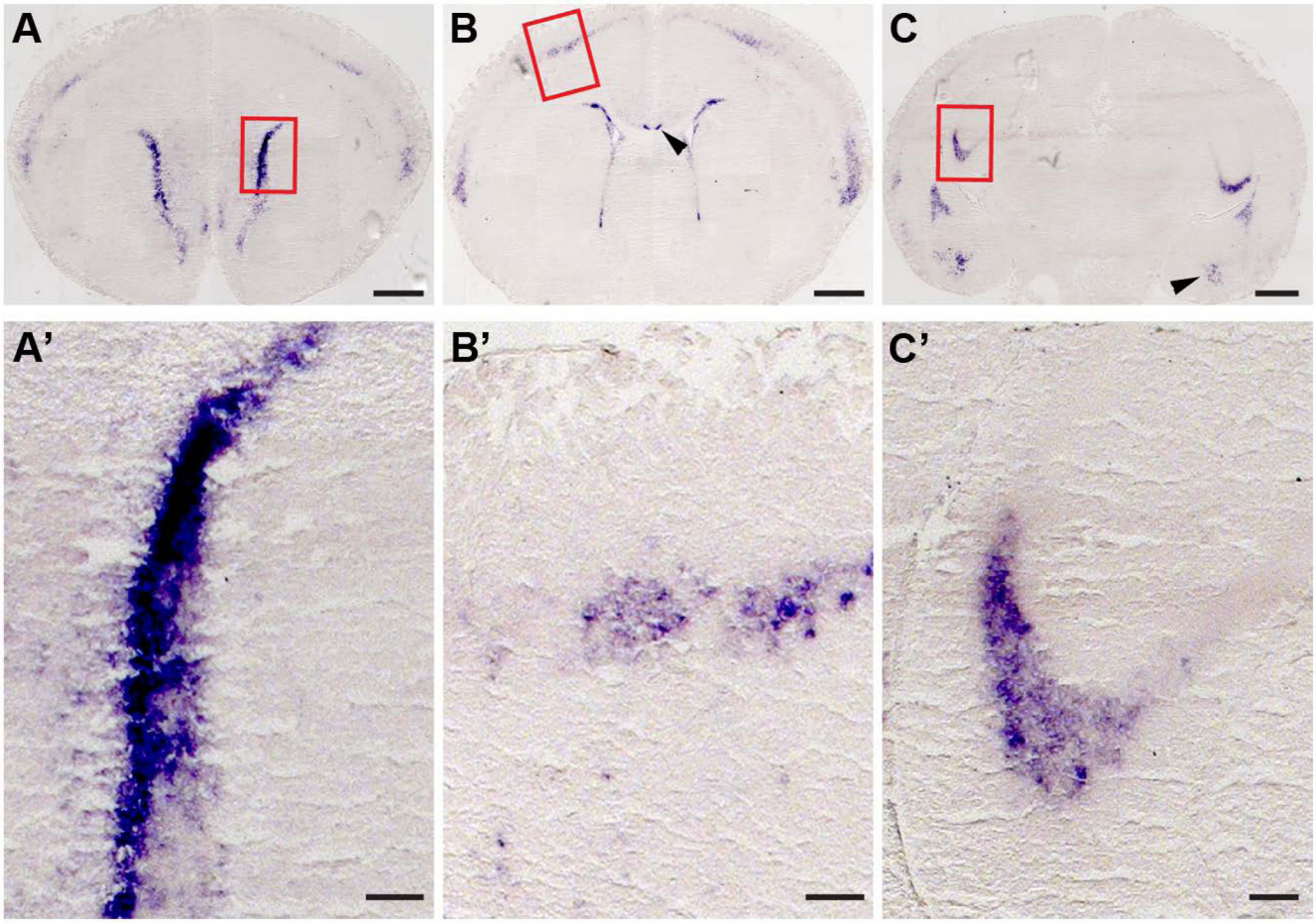

Figure 2.

Photomicrographs illustrate the distribution of *hgf* mRNA in coronal sections through the P14 mouse forebrain. ***A–C***, low magnification view through different rostro-caudal levels. ***A'–C'***, represent higher magnification view of boxed area in A–C, respectively. There is robust signal in periventricular zones of the lateral ventricles (***A, A'***). *hgf* also is expressed in deep layers of the neocortex in a lateral-medial gradient (***A, B, B'***) and CA3 of the hippocampus (***C, C'***). Signal also is detected in the indusium griseum (arrowhead in ***B***) and basolateral amygdala (arrowhead in ***C***). Scale bar, 1mm (***A–C***); 125 μm (***A'–C'***).

Author Manuscript Author Manuscript Author Manuscript Author Manuscript

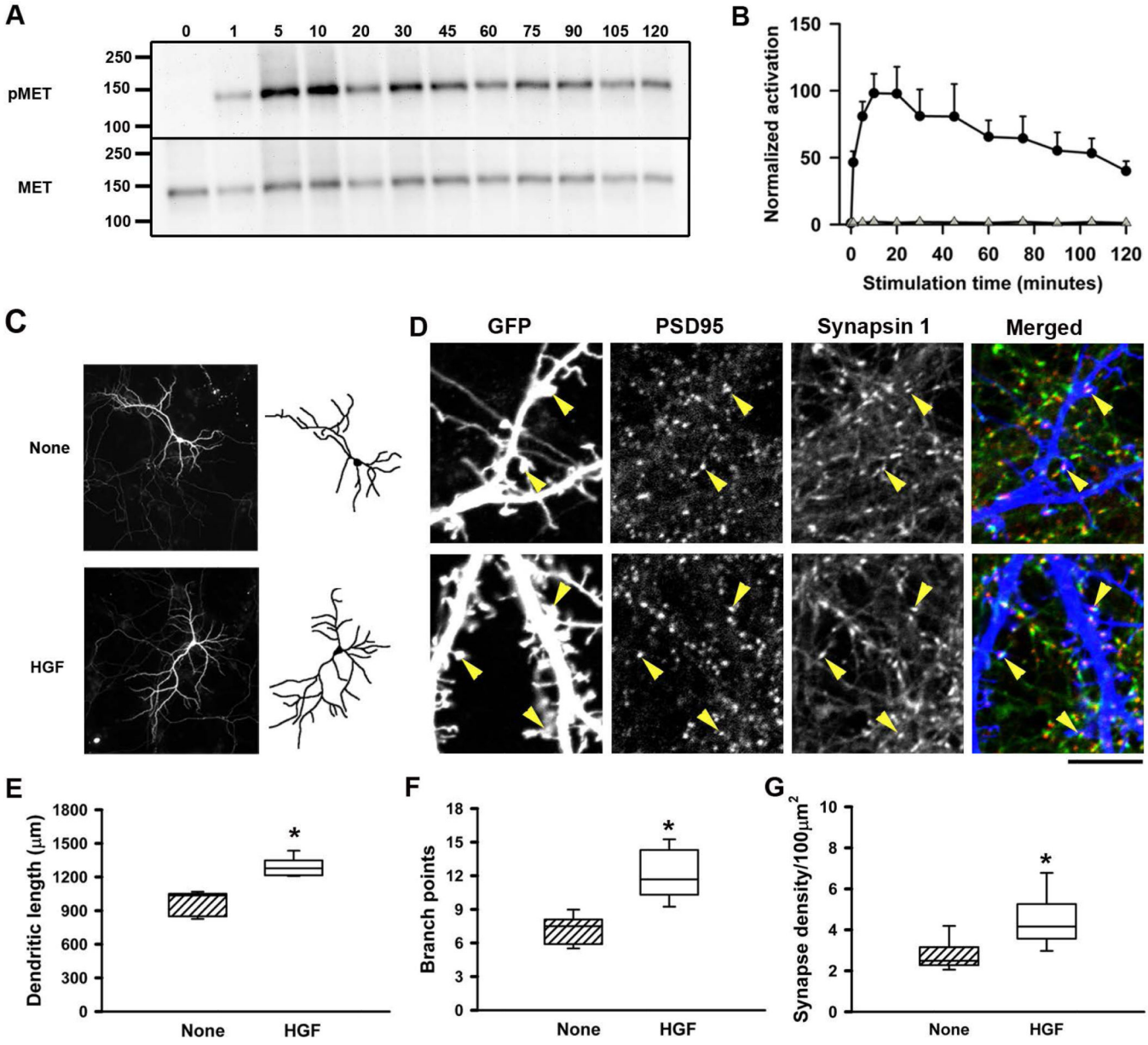

Figure 3.

HGF stimulation increases dendritic growth of and synapse density on neocortical neurons *in vitro* ***A***, Representative Western blot of MET phosphorylated at Tyr1234/1235 (pMET) following stimulation of neocortical cultures with HGF (50ng/ml) for 1–120 minutes at 13 DIV. ***B***, Quantification of HGF-induced MET activation at 13 DIV. pMET levels were normalized to total MET and data expressed relative to vehicle-treated cultures (0). Graph shows mean pMET levels ± SEM. N=3 independent culturing sessions. ***C***, Photomicrographs (left panel) and reconstruction (middle panel) of GFP-expressing cortical neurons at 13–14 DIV following treatment with 0 or 50ng/ml HGF for 24 hours. Scale bar, 200 μm. ***D***, Confocal images illustrating GFP (blue in merged), PSD95 (red in merged) and synapsin-1 (green in merged) immunoreactivity at 13 −14 DIV following treatment with 0 or 50ng/ml HGF for 24 hours. Arrowheads indicate congruent GFP, PSD95 and synapsin 1

Author Manuscript Author Manuscript Author Manuscript Author Manuscript

signal. Scale bar, 10μm. Total dendritic length (**E**), number of branch points (***F***) and synapse density (***G***) were quantified and data presented as box (striped boxes, 0ng/ml HGF; white boxes, 50ng/ml HGF) and whisker plots. The box represents the 25th and 75th percentiles and the whiskers denote the 5th and 95th percentiles. The line bisecting each box is the median. *$p < 0.05$ by two-tailed t-test (N=7 pups from 2 separate culturing sessions).

Author Manuscript Author Manuscript Author Manuscript Author Manuscript

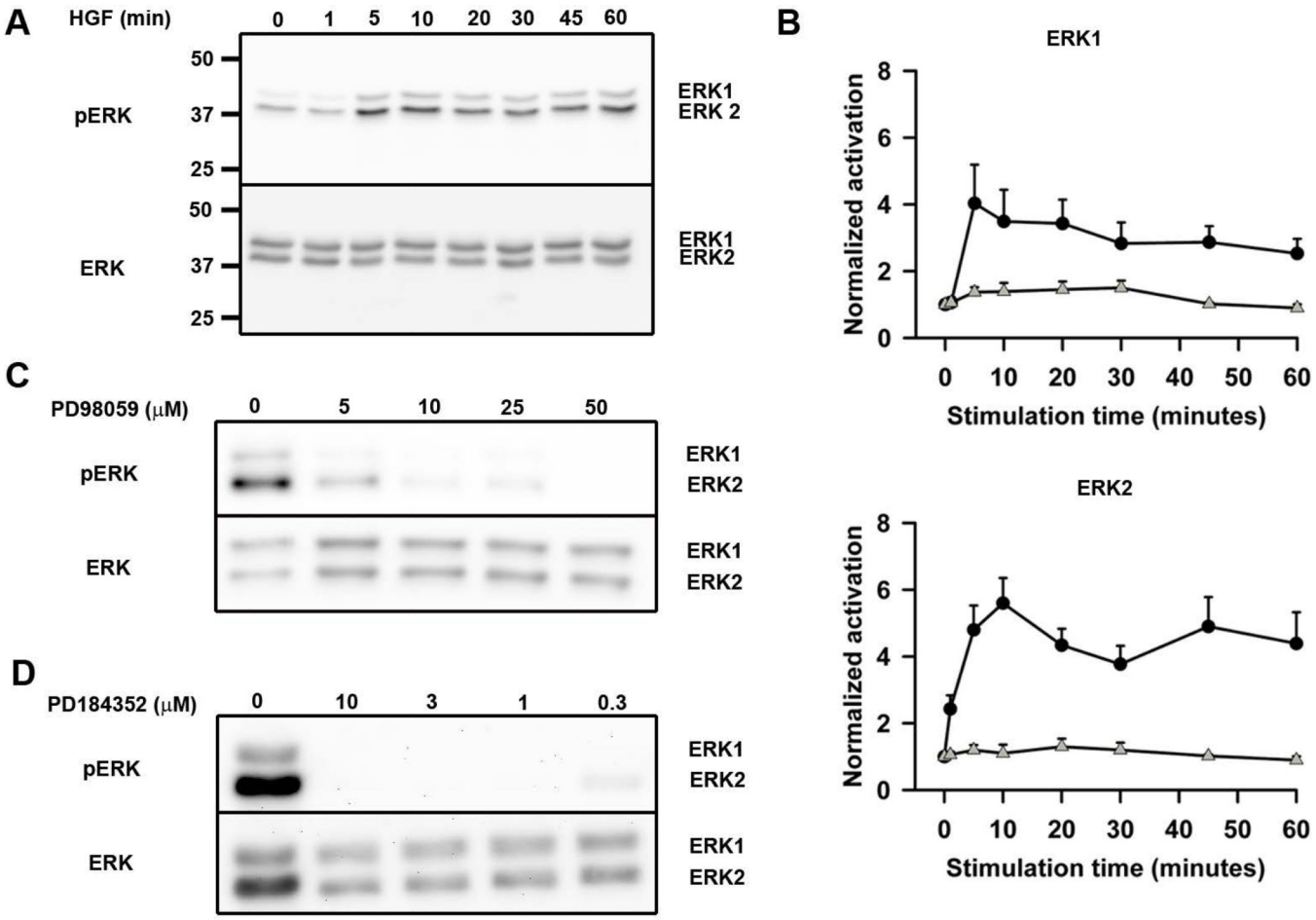

Figure 4.

HGF-induced activation of ERK in neocortical neurons in vitro. ***A***, Representative Western blot of ERK1/2 phosphorylated at Thr202/Tyr204 (pERK) following stimulation of neocortical cultures with HGF (50ng/ml) for 1–60 minutes at 13 DIV. ***B***, Quantitative analysis of HGF-induced ERK phosphorylation in response to HGF (black circles, 50ng/ml HGF; gray triangles, 0ng/ml HGF). pERK levels were normalized to total ERK and data expressed relative to vehicle-treated cultures (0). Graphs shows mean pERK1 and pERK2 levels ± SEM. N=3 independent culturing sessions. ***C, D***, Inhibition of HGF-induced ERK phosphorylation in vitro. Representative Western blots showing the effect of different concentrations of PD98059 (***C***) and PD 184352 (***D***) on ERK1/2 phosphorylation after HGF treatment for 30 minutes. 25μM PD98059 and 1μM PD 184352 were used in subsequent assays.

Author Manuscript Author Manuscript Author Manuscript Author Manuscript

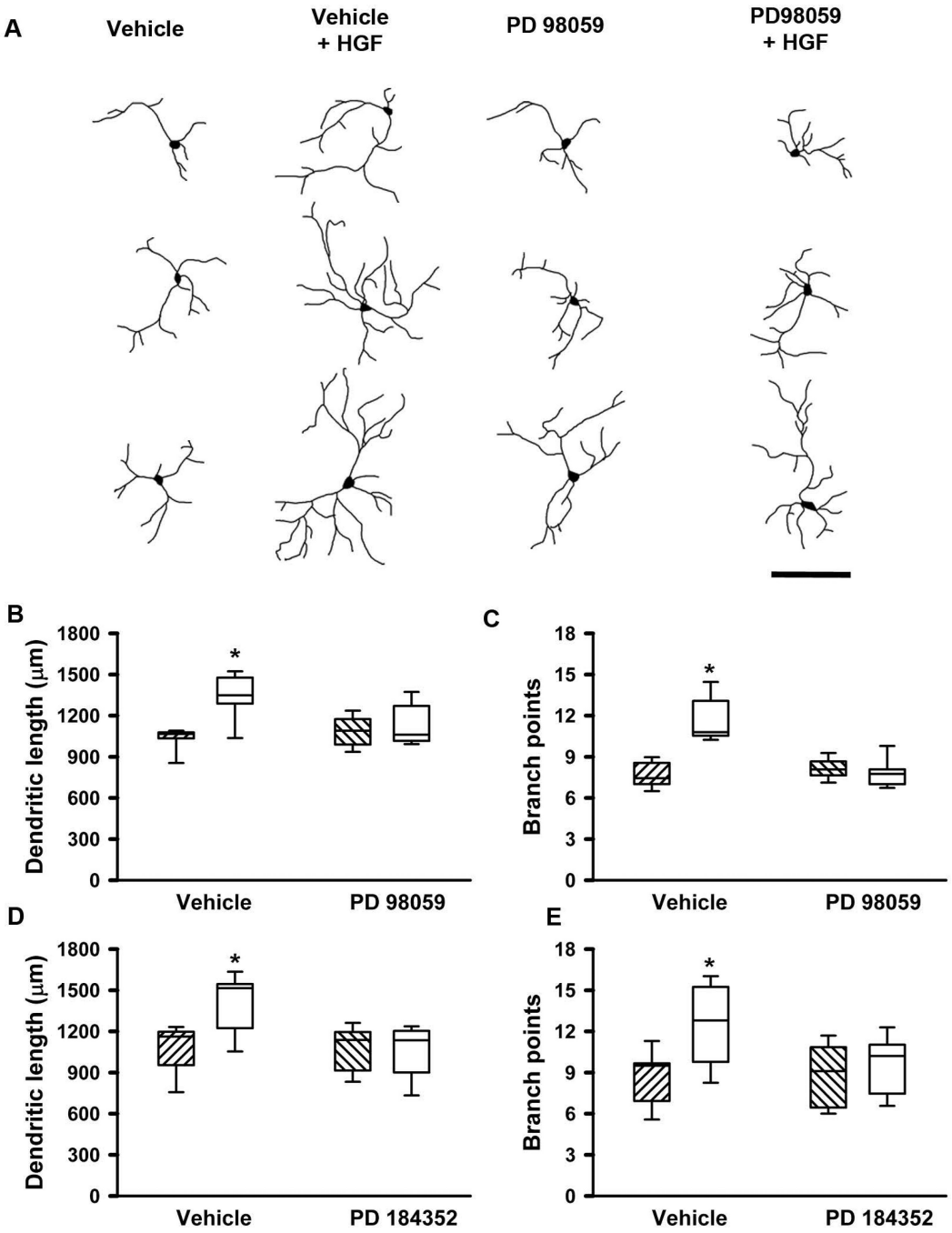

Figure 5.

HGF increases dendritic growth of neocortical neurons through the ERK1/2 pathway. ***A***, Reconstructed dendritic arbors of GFP-expressing cortical neurons at 13–14 DIV representing neurons in the 25th (top row), 50th (middle row) and 75th (bottom row) percentile of the sampled populations following treatment with 0 or 50ng/ml HGF in the presence of vehicle or inhibitor for 24 hours. Scale bar, 200 μm. ***B–E***, Quantification of the effects of PD98059 (***B, C***) and PD 184352 (**D, E**) on dendritic growth. Total dendritic length (***B, D***) and number of branch points (**C, E**) were quantified and data presented as a box

Author Manuscript Author Manuscript Author Manuscript Author Manuscript

(striped boxes, 0ng/ml HGF; white boxes, 50ng/ml HGF) and whisker plots. The box represents the 25th and 75th percentiles and the whiskers denote the 5th and 95th percentiles. The line bisecting each box is the median. For both measures, there is a significant interaction between HGF and inhibitor by two-way ANOVA. *$p < 0.05$ compared to all other groups by Tukey's HSD (N=7 pups from 2 separate culturing sessions).

Author Manuscript Author Manuscript Author Manuscript Author Manuscript

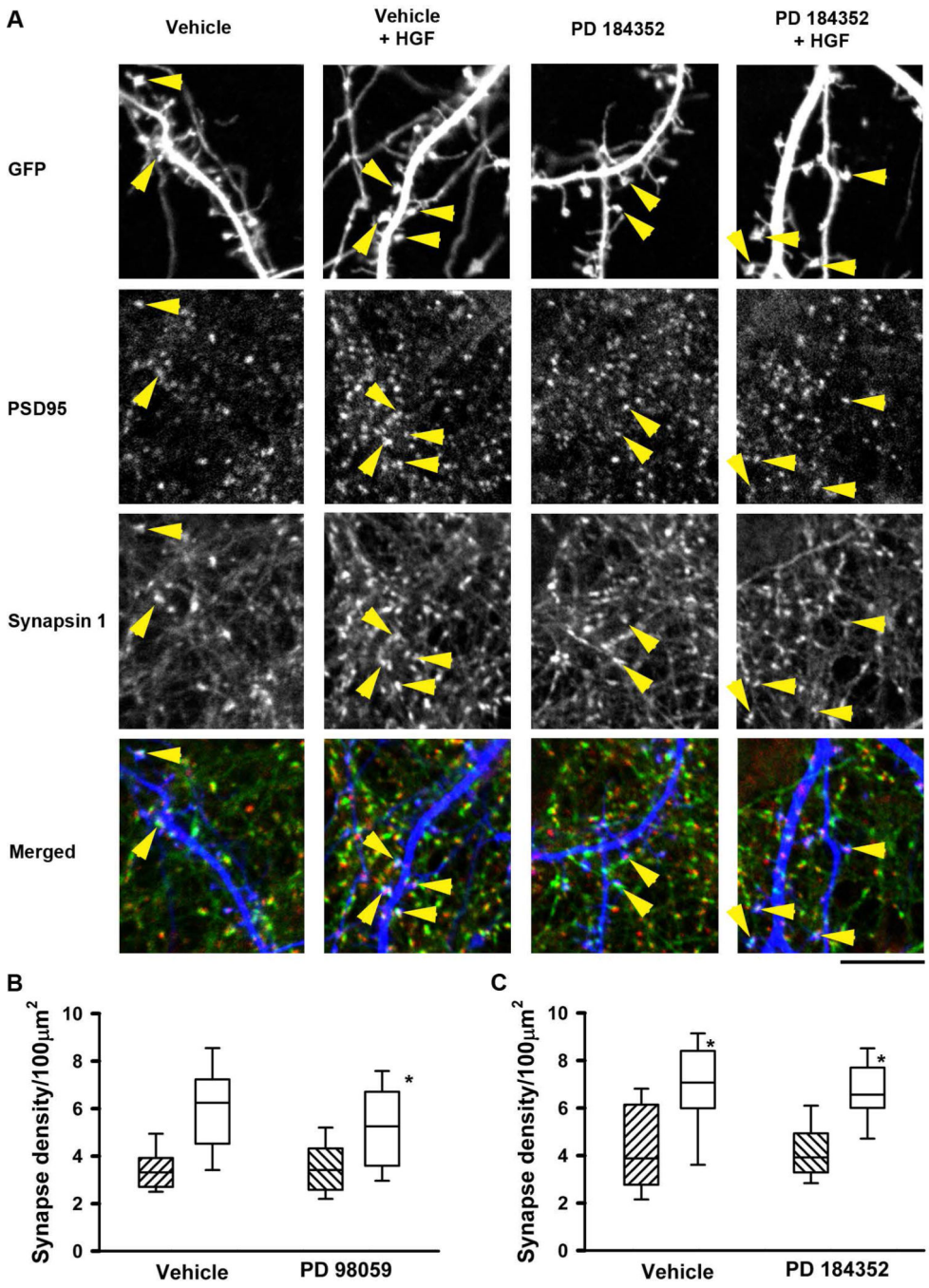

Figure 6.

Inhibition of the ERK1/2 pathway has no effect on HGF-induced synapse density. ***A***, Confocal images illustrating GFP (blue in merged), PSD95 (red in merged) and synapsin-1 (green in merged) immunoreactivity at 13–14 DIV following treatment with 0 or 50ng/ml HGF in the presence of vehicle or inhibitor for 24 hours. Arrowheads indicate congruent GFP, PSD95 and synapsin 1 signal. Scale bar, 10μm. ***B, C***, Quantification of the effects of PD98059 (***B***) and PD 184352 (**C**) on synapse density. The data are presented as a box (striped boxes, 0ng/ml HGF; white boxes, 50ng/ml HGF) and whisker plot, with the box

representing the 25th and 75th percentiles and the whiskers denoting the 5th and 95th percentiles. The line bisecting each box is the median. There is a significant main effect of HGF (*$p < 0.05$), but no main effect of PD98059 or PI 184352 by two-way ANOVA (N=7 pups from 2 separate culturing sessions).

Author Manuscript Author Manuscript Author Manuscript Author Manuscript

Author Manuscript Author Manuscript Author Manuscript Author Manuscript

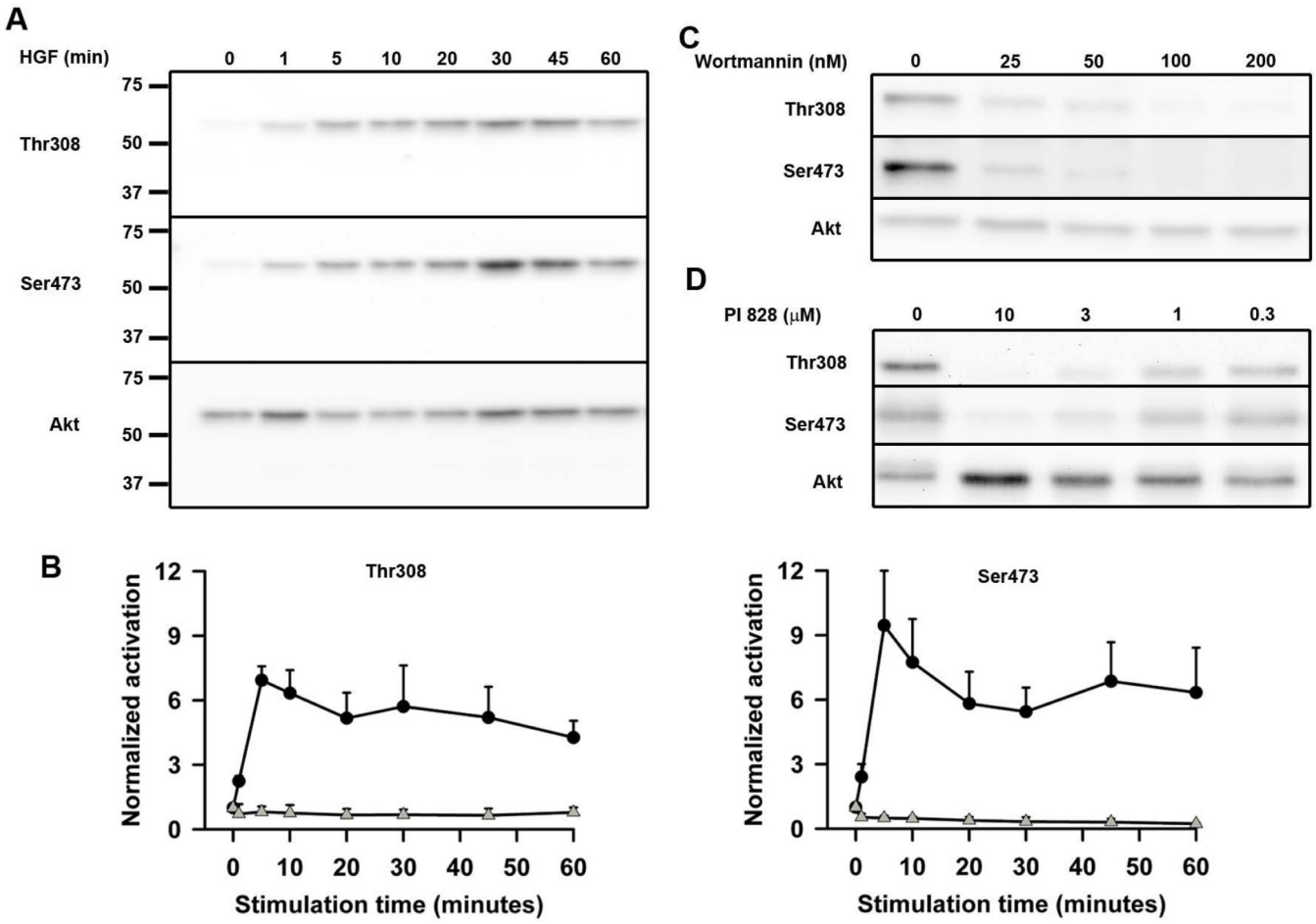

Figure 7.

HGF-induced activation of Akt in neocortical neurons in vitro. ***A***, Representative Western blots of Akt phosphorylated at Thr308 and Ser473 following stimulation of neocortical cultures with HGF (50ng/ml) for 1–60 minutes at 13 DIV. ***B***, Quantitative analysis of HGF-induced Akt phosphorylation in response to HGF (black circles, 50ng/ml HGF; gray triangles, 0ng/ml HGF). pAkt levels were normalized to total Akt and data expressed relative to vehicle-treated cultures (0). Graphs show mean pAkt levels ± SEM. N=3 independent culturing sessions. ***C, D***, Inhibition of HGF-induced Akt phosphorylation in vitro. Representative Western blot showing the effects of different concentrations of wortmannin (**C**) and PI 828 (**D**) on Akt phosphorylation after HGF treatment for 30 minutes. 100nM wortmannin and 3μm PI828 were used in subsequent assays.

Author Manuscript Author Manuscript Author Manuscript Author Manuscript

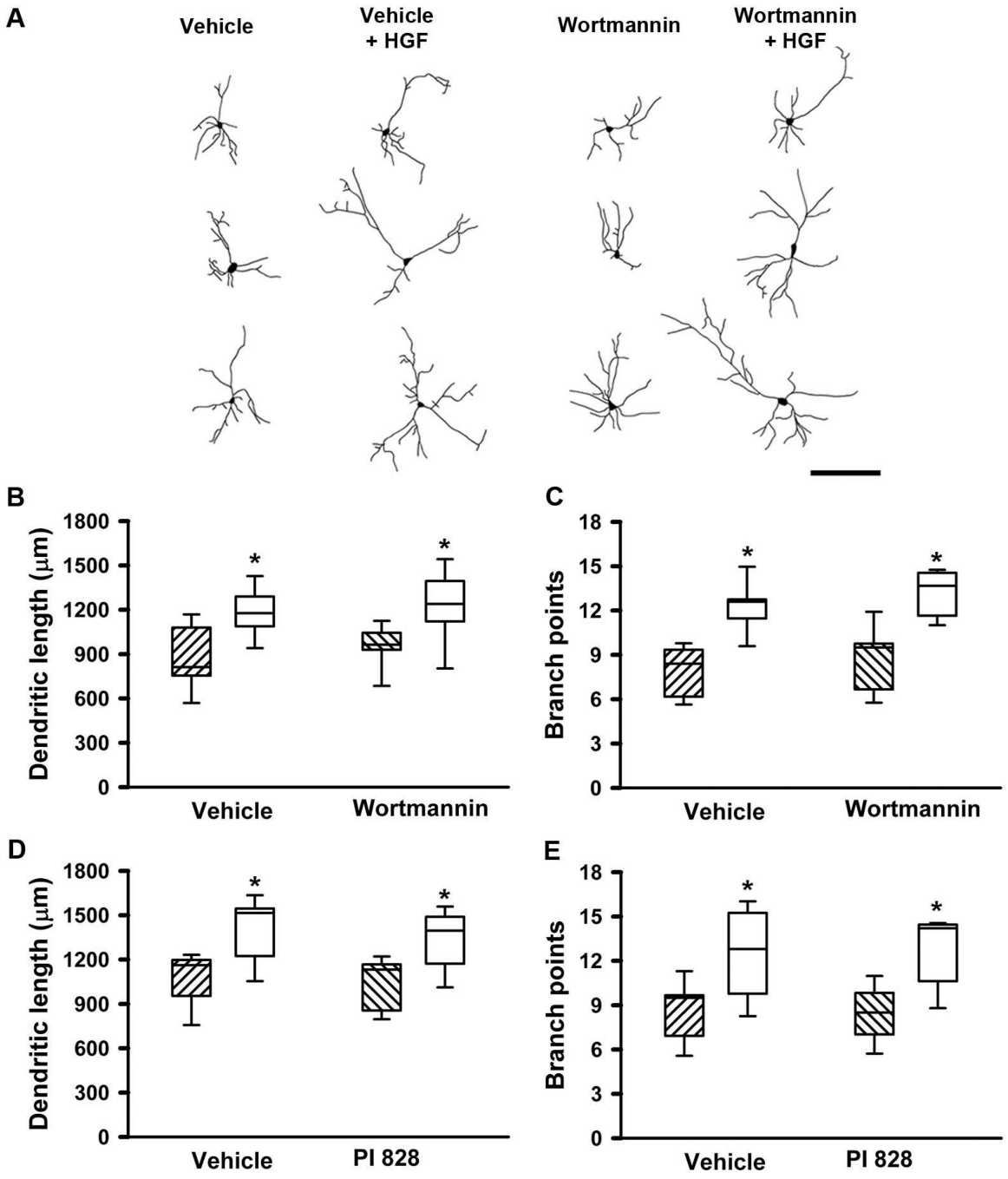

Figure 8.

Inhibition of the PI-3K/Akt pathway has no effect on HGF-induced synapse density.***A***, Reconstructed dendritic arbors of GFP-expressing cortical neurons at 14 DIV representing neurons in the 25th (top row), 50th (middle row) and 75th (bottom row) percentile of the sampled populations following treatment with 0 or 50ng/ml HGF in the presence of vehicle or inhibitor for 24 hours. Scale bar, 200 μm. ***B-E***, Quantification of the effects of wortmannin (***B, C***) and PI 828 (**D, E**) on dendritic growth. Total dendritic length (***B, D***) and number of branch points (***C, E***) were quantified and data presented as a box (striped boxes,

Author Manuscript Author Manuscript Author Manuscript Author Manuscript

0ng/ml HGF; white boxes, 50ng/ml HGF) and whisker plots. Note that the vehicle data for PI 828 are the same data set as used in Figure 5. The box represents the 25^{th} and 75^{th} percentiles and the whiskers denote the 5^{th} and 95^{th} percentiles. The line bisecting each box is the median. For both measures, there is a significant main effect of HGF (*$p < 0.05$), but no main effect of wortmannin or PI 828 by two-way ANOVA (N=7 pups from 2 separate culturing sessions).

Author Manuscript Author Manuscript Author Manuscript Author Manuscript

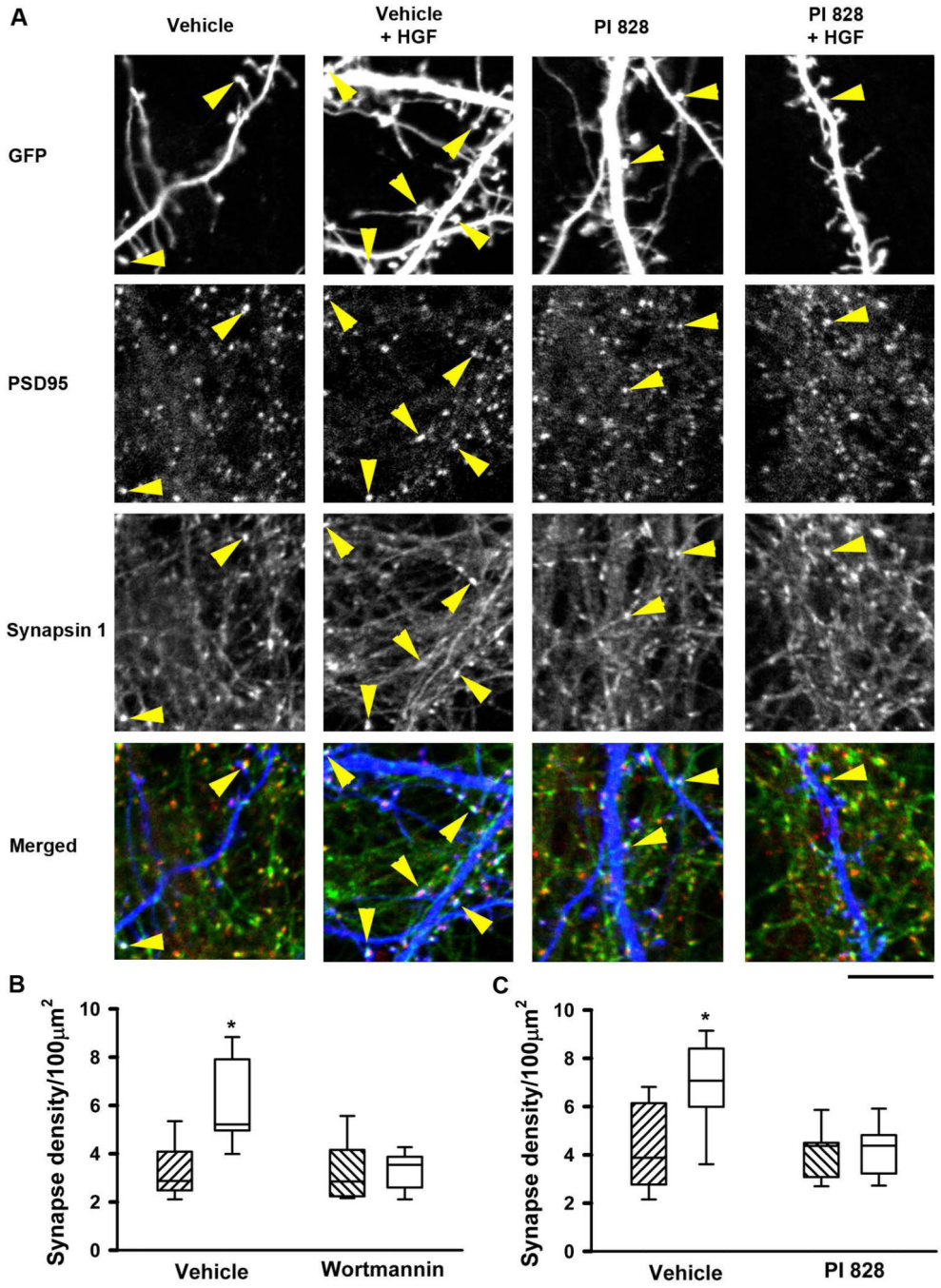

Figure 9.

HGF increases synapse density on neocortical neurons through the PI-3K/Akt pathway. ***A***, Confocal images illustrating GFP (blue), synapsin-1 (green), and PSD95 (red) immunoreactivity at 13–14 DIV following treatment with 0 or 50ng/ml HGF in the presence of vehicle or inhibitor for 24 hours. Arrowheads indicate congruent GFP, PSD95 and synapsin 1 signal. Scale bar, 10μm. ***B, C***, Quantification of the effects of wortmannin (***B***) and PI 828 (**C**) on synapse density. The data are presented as a box (striped boxes, 0ng/ml HGF; white boxes, 50ng/ml HGF) and whisker plot, with the box representing the 25th and

Author Manuscript Author Manuscript Author Manuscript Author Manuscript

75th percentiles and the whiskers denoting the 5th and 95th percentiles. Note that the vehicle data for PI 828 are the same data set as used in Figure 5. The line bisecting each box is the median. There is a significant interaction between HGF and inhibitor by two-way ANOVA. *$p < 0.05$ compared to all other groups by Tukey's HSD (N=7 pups from 2 separate culturing sessions).

Author Manuscript Author Manuscript Author Manuscript Author Manuscript

Table 1

Post-hoc analyses of age-related changes in pMET activation

	P7	P10	P14	P17	P18	P19	P20	P21	P28
P0	0.116	0.360	0.468	0.043	0.008	0.005	0.005	0.001	0.002
P7		0.022	0.448	0.001	<0.001	<0.001	<0.001	<0.001	<0.001
P10			0.131	0.308	0.078	0.059	0.057	0.019	0.023
P14				0.012	0.002	0.002	0.002	<0.001	0.001
P17					0.365	0.291	0.283	0.124	0.131
P18						0.885	0.872	0.586	0.555
P19							0.987	0.696	0.656
P20								0.709	0.667
P21									0.931

Author Manuscript Author Manuscript Author Manuscript Author Manuscript

Table 2

Post-hoc analyses of age-related changes in MET levels

	P7	P10	P14	P17	P19	P21	P28
P0	0.004	<0.001	0.062	0.219	0.911	0.632	0.476
P7		0.111	0.084	0.005	0.004	0.004	0.004
P10			0.340	<0.001	<0.001	<0.001	<0.001
P14				0.098	0.065	0.069	0.057
P17					0.303	0.386	0.174
P19						0.792	0.607
P21							0.428

Dev Neurobiol. Author manuscript; available in PMC 2017 October 01.

Author Manuscript
Author Manuscript
Author Manuscript
Author Manuscript

Table 3

Post-hoc tests of age-related changes in pMET levels

	P7	P10	P14	P17	P19	P21	P28
P0	<0.001	0.023	0.095	0.378	0.010	0.001	<0.001
P7		0.002	0.008	<0.001	<0.001	<0.001	<0.001
P10			0.837	0.016	0.014	0.013	0.011
P14				0.073	0.069	0.063	0.059
P17					0.635	0.217	0.078
P19						0.357	0.105
P21							0.355

Author Manuscript

Author Manuscript

Author Manuscript

Author Manuscript

Table 4

Post-hoc tests of effects of MAPK/ERK inhibitors on dendritic length

	Vehicle + HGF	Inhibitor alone	Inhibitor + HGF
A. PD98059			
Vehicle	0.002	0.393	0.177
Vehicle + HGF		0.008	0.040
Inhibitor alone			0.177
B. PD 184352			
Vehicle	0.012	0.920	0.854
Vehicle + HGF		0.012	0.010
Inhibitor alone			0.773

Author Manuscript

Author Manuscript

Author Manuscript

Author Manuscript

Table 5

Post-hoc tests of effects of MAPK/ERK inhibitors on number of branch points

	Vehicle + HGF	Inhibitor alone	Inhibitor + HGF
A. PD98059			
Vehicle	<0.001	0.328	0.805
Vehicle + HGF		<0.001	<0.001
Inhibitor alone			0.548
B. PD 184352			
Vehicle	0.017	0.671	0.548
Vehicle + HGF		0.029	0.037
Inhibitor alone			0.856

Author Manuscript

Author Manuscript

Author Manuscript

Author Manuscript

Table 6

Post-hoc tests of effects of PI3-K inhibitors on synapse density

	Vehicle + HGF	Inhibitor alone	Inhibitor + HGF
A. Wortmannin			
Vehicle	0.008	0.934	0.965
Vehicle + HGF		0.011	0.004
Inhibitor alone			0.965
B. PI828			
Vehicle	0.013	0.852	0.686
Vehicle + HGF		0.010	0.015
Inhibitor alone			0.797